SEDIMENTOLOGY the journal of the International Association of Sedimentologists

Sedimentology (2022) **69**, 501–536 doi: 10.1111/sed.12913

Drainage and environmental evolution across the Permo–Triassic boundary in the south-east Germanic Basin (north-east Bavaria)

DOMENICO C. G. RAVIDÀ* , LUCA CARACCIOLO*, SATURNINA HENARES† , MEIKE JANßEN* and HARALD STOLLHOFEN*

**GeoZentrum Nordbayern, Friedrich-Alexander-University (FAU) Erlangen-Nürnberg, Schlossgarten 5, Erlangen, 91054, Germany (E-mail: domenico.ravida@fau.de)*

†Department of Earth and Environmental Sciences, Division of Geology, KU Leuven, Celestijnenlaan 200E, Leuven, B-3001, Belgium

Associate Editor – Victoria Valdez

ABSTRACT

The identification of the factors triggering continental environmental changes at the Permian–Triassic transition is of general interest as they allow a better understanding of the most controversial mass extinction of the Phanerozoic. This study investigates the environmental response to external forcings on continental successions at the south-east-margin of the Central European Basin System in Germany. Studies from this area are scarce, and its evolution is poorly understood. This work integrates high-resolution core-logging and quantitative sedimentary petrography of Middle Permian–Early Triassic successions recovered from the wells Obernsees-1 and Lindau-1. The sedimentological investigation reveals major vertical variations in the depositional settings marked by changes in grain-size trends and facies associations: (i) the progradation of mass flow/fluvial fans over sandflat environments denotes the Guadalupian–Lopingian; (ii) sabkha to shallow-marine conditions occur during the uppermost Permian; (iii) the onset of braided fluvial sequences marks the Permian–Triassic boundary; (iv) changes in fluvial style, reflecting increased river sinuosity, and aeolian deposition characterize the remaining Triassic. Environmental changes are accentuated by variations in sediment composition. Proximal deposits (for example, alluvial fan) are lithic arkoses, while more distal associations reveal arkosic composition. Detrital modes point to: (i) a high-grade metamorphic source feeding the drainage of Lindau-1 (metamorphic index, MI 441–500); and (ii) a mixed low-grade and high-grade metamorphic source (MI 277–395) feeding the Permian of Obernsees-1, passing upward to high-grade metamorphic (MI 441–500) and subordinate granitoid sources. Compositional signatures and environmental changes suggest distinct drainage evolutions regulated by upstream climate and tectonic controls. The higher plutonic clast content coeval to the onset of fluvial sedimentation and coarse-grained influxes reflects local tectonic perturbations attributed to the Early Triassic reactivation of Variscan faults. The evidence of perennial fluvial systems during the lowermost Triassic reflects wetter climate conditions in the upstream catchment area, which contradicts the common view of increased aridity at the Permian–Triassic boundary.

Keywords Central European Basin Systems, Early Triassic climate, external forcing controls, fluvial sedimentology, Permo–Triassic boundary, provenance analysis, synsedimentary tectonics.

INTRODUCTION

The Permian–Triassic Boundary (PTB) witnessed the most devastating Phanerozoic mass extinction (Erwin, 1994; Hallam & Wignall, 1997). About 95% of marine species and 75% of terrestrial species, both plants and animals, went extinct (Jin *et al.*, 2000; Song *et al.*, 2013). Drastic environmental changes occurred worldwide, both in oceans and on land (Ward *et al.*, 2000; Benton & Newell, 2014). Several models have been established to explain causes leading to the biosphere collapse and environmental changes, most of them relating to effects of the Siberian trap volcanism (Renne *et al.*, 1995; Burgess *et al.*, 2017; Black *et al.*, 2018) and enhanced global warming (Kidder & Worsley, 2004; Joachimski *et al.*, 2012, 2020; Sun *et al.*, 2012). General models for continental sedimentation converge towards increasing mass wasting and aridity across the Permian–Triassic transition, together with a potential increase of sediment flux and change in fluvial styles (Algeo & Twitchett, 2010; Benton & Newell, 2014). Triassic braided rivers gradationally or abruptly follow on Late Permian playa and meandering systems in many regions: South Africa (Smith, 1995; Ward *et al.*, 2000; Viglietti *et al.*, 2017), Russia (Newell *et al.*, 1999; Newell *et al.*, 2010; Kearsey *et al.*, 2012), China (Chu *et al.*, 2016; Zhu *et al.*, 2020), India (Sarkar *et al.*, 2003; Mishra *et al.*, 2018), Poland (Jewuła *et al.*, 2020a) and France (Bourquin *et al.*, 2006). Newell *et al.* (1999) and Ward *et al.* (2000) linked this change to a massive die-off event of rooted plants, promoting riverbank erosion and multichannel braiding processes (Schumm, 1985). However, some authors challenged such a significant biosphere turnover (Gastaldo *et al.*, 2009; Nowak *et al.*, 2019). Relatively new studies report an increase in exhumation rates (Charton *et al.*, 2020) and global sediment flux in relation to climate and enhanced chemical weathering of soils and bedrocks contemporaneous to the PTB (Algeo & Twitchett, 2010; Algeo *et al.*, 2011; Cao *et al.*, 2019). Whether sediment production increased, and what the potential causes could have been, is still a matter of debate. While on the one hand, the exiguous number of complete continental sections crossing the PTB limits the palaeoclimate research, on the other hand, the effects of local tectonism are often neglected.

Previous studies on the terrestrial PTB in Europe have focused on the effects of regional tectonism and eustasy on the sedimentary evolution in the Central European Basin System (CEBS) (Aigner & Bachmann, 1992; Aigner *et al.*, 1999; Geluk, 2005; Geluk & Röhling, 2016). Little attention has been given to the environmental response and global implications of the biosphere collapse (Scholze *et al.*, 2017; Jewuła *et al.*, 2020b) and climate changes (Péron *et al.*, 2005; Bourquin *et al.*, 2009). The persistence of lacustrine settings across the PTB described by Hiete *et al.* (2006) in the North CEBS reflects a positive shift in the water balance against the global tendency of hyper-arid climate. Increased water discharge from the more humid Hercynian reliefs surrounding the CEBS has also been discussed by Péron *et al.* (2005) and Bourquin *et al.* (2009) and matches the increase in precipitation described in several models (Parrish, 1993; Retallack, 2013).

This paper investigates the Permian – lower Triassic sedimentary infill of the SE–CEBS in Germany (Franconian Basin – Fig. 1). Compared to other Permian–Triassic basins, information on this area is scarce. However, the good preservation of the sedimentary sequences provides a great opportunity for understanding the effect of external forcing controls on the environmental evolution across the PTB. Frequent changes in facies associations marked by grain-size cycles, accentuated in the Bohemian Massif (BM) proximity, have been described for the Franconian Basin (Freudenberger & Schwerd, 1996). Even though the controls on sedimentation are still debated, several studies support a tectonic influence, induced by the reactivation of north-west/south-east-striking Variscan faults (Klare, 1989; Zulauf, 1993; Mattern, 1995a,b; Peterek *et al.*, 1997; Schröder *et al.*, 1997), either in compressional or extensional regimes, and neglect the effects of climate perturbations. This paper explores the successions recovered from the wells Obernsees-1 and Lindau-1 (Fig. 2). Detailed facies analysis and petrographic composition are integrated to: (i) investigate the role of external forcing controls on the palaeodrainage modifications and changes in fluvial style across the PTB; (ii) identify drainages and sediment sources; and (iii) reconstruct the lateral evolution of the depositional environment.

GEOLOGICAL SETTING

Tectonic, climate and sediment source

The term Franconian Basin relates to a south-west/north-east-trending depositional area

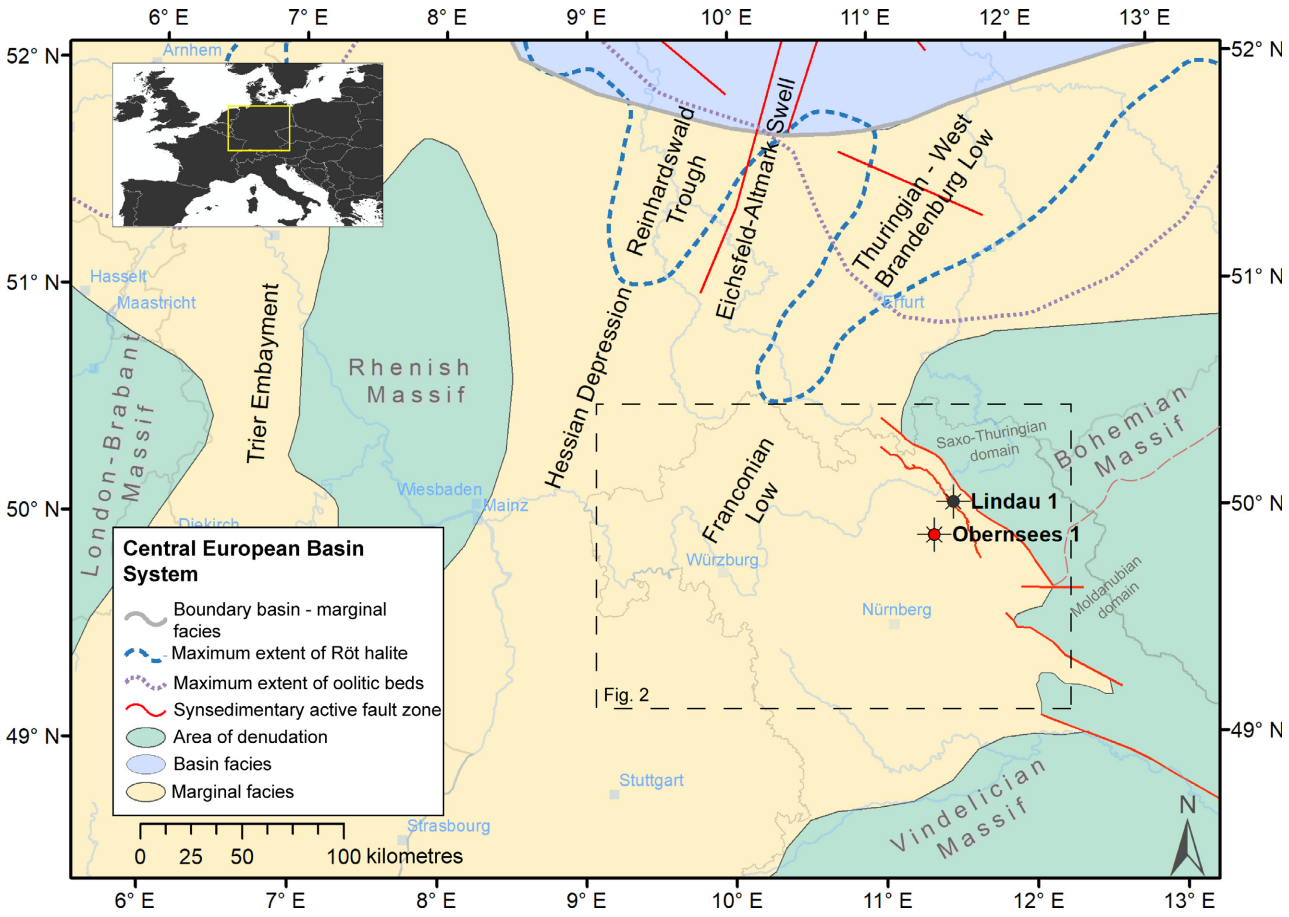

Fig. 1. Palaeogeography of the Central European Basin Systems (CEBS) (after Hiete *et al.*, 2006). The rectangle shows the position of the maps in Fig. 2.

occupying the south-east margin of the CEBS in south-east Germany (Fig. 1), filled with Late Permian (Zechstein) to Jurassic strata (Freudenberger & Schwerd, 1996) and overlying older structurally-controlled Carboniferous–Permian basin configurations (Fig. 2A). The Franconian Basin is east-bounded by the BM, the most significant exposure of Variscan basement rocks in Central Europe and considered the primary sediment source of the SE–CEBS (Schröder *et al.*, 1997; Dill & Klosa, 2011; Augustsson *et al.*, 2018, 2019). Two tectonostratigraphic domains are recognized along the western BM: (i) the Moldanubian terrain (SE BM) (Fig. 2) consisting of pre-Variscan paragneisses and granulites (Žák *et al.*, 2011) and metavolcanic/metasedimentary rocks; and (ii) the Saxo-Thuringian terrain (NW BM) consisting of Ediacaran plutonic and volcano-sedimentary rocks overlain by Cambrian to Early Carboniferous metasedimentary units and low to high-grade metamorphic series (Linnemann, 2007; Wall *et al.*, 2019). Several north-west/south-east-striking strike-slip faults (for example, *Franconian Line*, *Kulmbach Fault, Danube Fault and Pfahl Fault*) (Fig. 2) bound the BM to the west (Western Border fault Zone – WBZ, Peterek *et al.*, 1997) and controlled the development and filling of Late Carboniferous transtensional basins (Meyer, 1989; Mattern, 1995b; Schröder *et al.*, 1997). Amongst these, the south-west/north-east *Kraichgau* Basin extends under most of the Franconian Basin and spreads further into south-west Germany (Meschede & Warr, 2019). The north-west/south-east *Naab* Basin forms a narrow pull-apart structure along the western footwall of the BM (Müller, 1994) (Fig. 2A). The hydrological connection between the two basins is still unclear (Helmkampf, 2006; Paul, 2006). Rotliegend siliciclastic deposits (Roadian–Wuchiapingian) represent the first post-Variscan basin infill (Fig. 3). Deposition occurred under increasingly semiarid

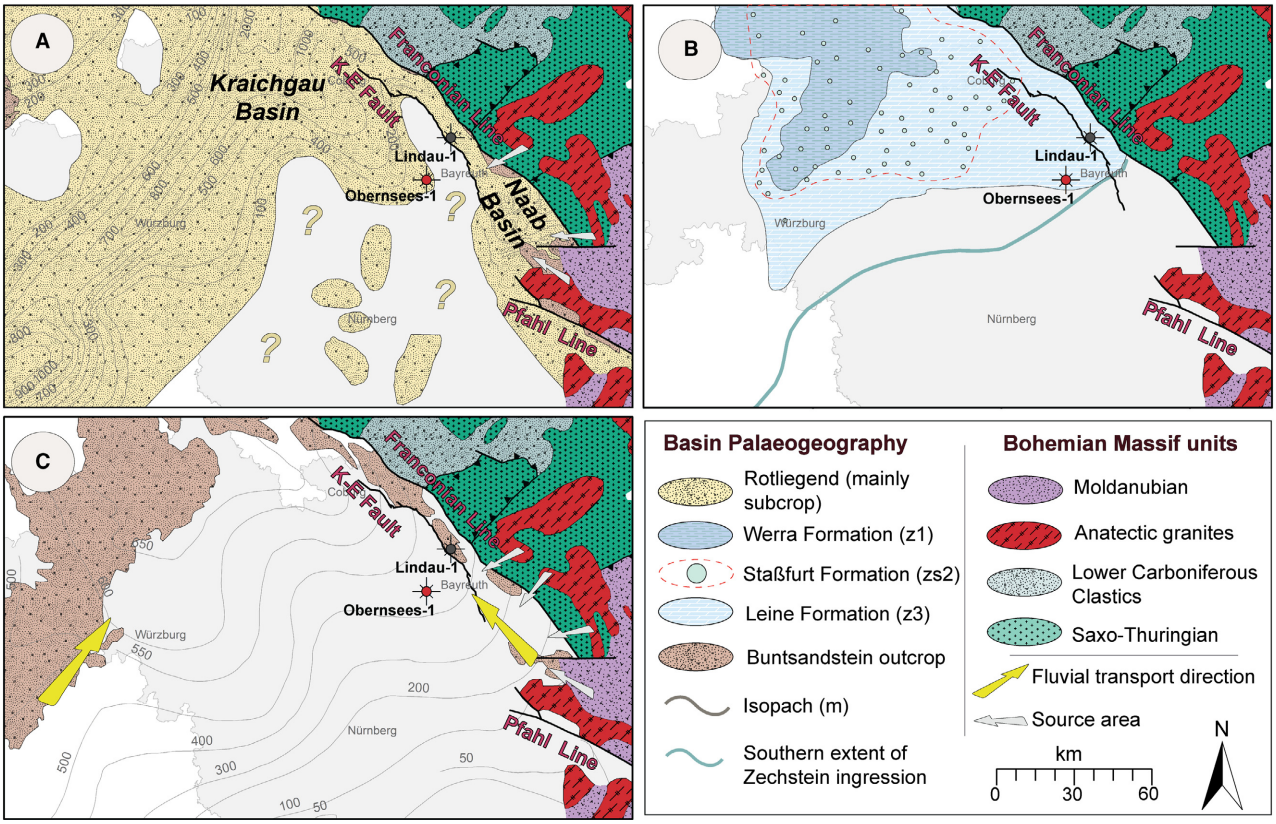

Fig. 2. Palaeogeography of the Franconian Basin during the deposition of: (A) Rotliegend; (B) Zechstein; and (C) Buntsandstein (compiled from Freudenberger & Schwerd, 1996). The Bohemian Massif terrains are shown to the East (Linnemann, 2007). K-E: Kulmbach–Eisfeld Fault (Wall *et al.*, 2019). Question marks in (A) indicate regions of uncertainty where Rotliegend beds are not proven by drilling but cannot be ruled out (Paul, 2006). Bavarian borders outlined in light-grey colour. Yellow arrows in (C) are the main fluvial transport directions within the basin (Freudenberger *et al.*, 2014). Grey arrows in (A) and (C) indicate the sources of sediments according to Schröder *et al.* (1997).

to arid climate (Roscher & Schneider, 2006), favouring widespread desert-like and sabkha strata underlying alluvial fan beds in the most proximal regions (Freudenberger & Schwerd, 1996).

Several southward marine transgressions from the Arctic–North Atlantic Oceans affected the CEBS (Ziegler, 1990) during the uppermost Permian. The barren climate triggered intense evaporation processes (Summerhayes, 2015) resulting in the deposition of the Zechstein (Wuchiapingian–Changhsingian) evaporitic cycles in flooded regions (Tucker, 1991) and increased precipitation over the continental area (Roscher & Schneider, 2006). The multiple Zechstein sea-ingressions are only partially recorded in the Franconian Basin, where marginal siliciclastic facies frequently replace evaporitic marine strata (Schuh, 1985; Freudenberger *et al.*, 2016) (Fig. 2B).

A pronounced regressive tendency leading to deposition of the continental Buntsandstein redbeds (Induan–Anisian) marks the PTB (Aigner *et al.*, 1999; Bachmann *et al.*, 2008). The gradual southward enlargement of the Franconian Basin led to the deposition of the Buntsandstein onto the Zechstein or unconformably on the Upper Rotliegend and crystalline basement (Freudenberger & Schwerd, 1996). The result is a wedge-shaped basin architecture with a northwestward increasing thickness (Fig. 2C). The Buntsandstein is subdivided into Lower, Middle and Upper subgroups, based on unconformities, facies changes and internal sedimentary cycles (Aigner & Bachmann, 1992). Deposition occurred under arid climate with lack of seasonal precipitation (Péron *et al.*, 2005). From the

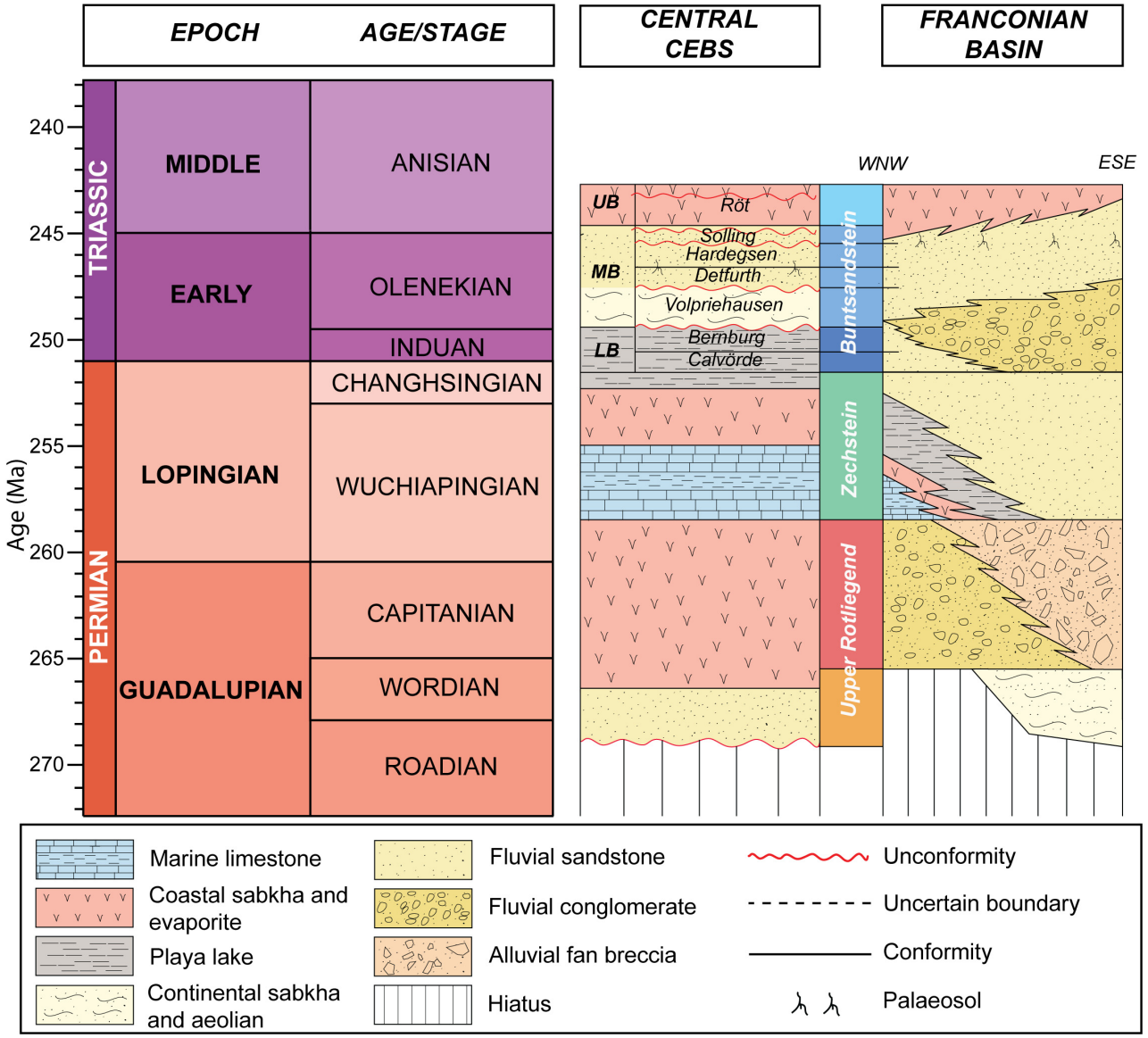

Fig. 3. Comparison of the Permian to lower Triassic sedimentary record between the distal portion of the Central European Basin Systems (CEBS) (modified from Bourquin *et al.*, 2011) and the Franconian Basin (compiled from Freudenberger & Schwerd, 1996; Upper Rotliegend stratigraphic attribution after Soffel & Wippern, 1998). Time-scale and stratigraphic chart from the International Commission of stratigraphy (Gradstein *et al.*, 2008). LB, Lower Buntsandstein; MB, Middle Buntsandstein; UB, Upper Buntsandstein.

investigation of the Buntsandstein palaeosols recorded in the well Obernsees-1, Weber (1993) compares the Franconian Basin to the modern semidesert of the South African Karoo and Kalahari regions. However, wetter conditions are indicated on the Hercynian reliefs surrounding the CEBS (Péron *et al.*, 2005; Bourquin *et al.*, 2009). In contrast to the sabkha–aeolian–ephemeral fluvial tendency of the central portions of the CEBS (Stollhofen *et al.*, 2008), coarse-grained fluvial systems developed in the Franconian Basin during the Lower–Middle Buntsandstein (Fig. 3). Freudenberger *et al.* (2014) report two dominant sediment transport directions in the basin: a north-eastern-transport in the western Franconian Basin and a north-western-transport parallel to the BM footwall (Fig. 2C). The increased discharge of coarse-grained sediments during the Buntsandstein is attributed to the reactivation of the WBZ leading to uplift and erosion of the western BM (Schröder, 1987; Klare, 1989; Mattern, 1995a;

Peterek *et al.*, 1997; Siebel *et al.*, 2010) (Fig. 2C). A retrogradation tendency characterizes the Middle–Upper Buntsandstein of the Franconian Basin, coupled with decreased tectonism (Peterek *et al.*, 1997). Widespread pedogenically overprinted meandering floodplain deposits (Olsen, 1988; Bindig & Backhaus, 1995) overlain by gypsum-rich sabkha beds form the dominant association (Freudenberger & Schwerd, 1996).

The Permian–Triassic strata discussed in this paper cover the Upper Rotliegend infill of the *Kraichgau* and *Naab* sub-basins and the Zechstein–Buntsandstein deposits of the overlying Franconian Basin recorded in the wells Obernsees-1 and Lindau-1 (Fig. 2). The lithostratigraphic subdivision of Obernsees-1 used herein (Fig. 4) includes the lithology-based interpretation of Emmert *et al.* (1985) and the magnetostratigraphic scheme of Soffel & Wippern (1998) for the Rotliegend–Zechstein interval. The subdivision of the Zechstein–Buntsandstein interval of Obernsees-1 considers more recent magnetostratigraphic (Szurlies, 2007) and lithological (Freudenberger *et al.*, 2014) schemes. The lithostratigraphic subdivision of Lindau-1 simply follows the gamma-ray-based scheme proposed by Helmkampf (2006) (Fig. 4).

SAMPLING AND METHODS

High-resolution sedimentary core descriptions were performed for the continuous cores of the wells Obernsees-1 (542.44 m) and Lindau-1 (530.6 m), logging grain-size variations, contacts, sedimentary structures and bed thicknesses. HCl *in situ* tests were performed for carbonate reactivity tests. The recognized lithofacies types (Table 1) were used to define the architectural elements and associated depositional settings following the coding of Miall (2006). The cores were digitized using the software WellCAD™. Ninety-nine samples were selected for petrographic analysis, thin sectioned, polished and treated for feldspar discrimination by staining with Na-cobaltnitrite (Chayes, 1952; Bailey & Stevens, 1960). A minimum of 300 framework components were counted for each thin section using the Gazzi-Dickinson point-count method (Ingersoll *et al.*, 1984; Zuffa, 1985). Metamorphic grains were classified following Garzanti & Vezzoli (2003). Confidence regions (95% and 99%) of detrital-mode means have been assessed following the procedure described in Aitchison (1997) and by computing log-ratio transformation of compositional data (Caracciolo *et al.*, 2014) using the 'R' package '*provenance*' (Vermeesch *et al.*, 2016).

LITHOFACIES ASSOCIATION AND EVOLUTION THROUGH THE PERMIAN–TRIASSIC BOUNDARY

The sedimentological analysis provided the basis for defining five lithofacies associations and interpreting eight depositional environments and type-sequences described below. Tables 1 and 2 summarize the main characteristics of each lithofacies and the interpreted depositional environment.

Breccia beds: mass flow/fluvial fan deposits

This lithofacies association is dominated by very poorly sorted reddish breccia deposits distinguished according to their massive nature (*Gmm* and *Gcm*) or the occurrence of internal stratification (*Gtp* and *Gh*). Clasts are angular to subangular and range from granules to cobbles. Massive deposits either display clasts floating in a Fe-rich clay/silt and subordinate very fine sandy matrix (lithofacies *Gmm*) or clast-supported matrix-rich texture (lithofacies *Gcm)* with weak normal to reverse grain-size grading (Fig. 5A and 5B). Basal boundaries are sharp but non-erosive, and bed thicknesses range between 0.3 to 4.0 m. High to low-angle planar and trough cross-bedded deposits (lithofacies *Gtp*) display sharp to erosive basal boundaries and weak clast imbrication. Thicknesses range between 0.1 to 0.9 m (Fig. 5C and 5D). Horizontal plane-bedded units (lithofacies *Gh*) are sharp-bounded with thicknesses varying between 0.1 to 0.3 m. Massive claystone/siltstone deposits (lithofacies *Fm*) locally occur interbedded (0.08 to 0.6 m thick), often exhibiting pedogenic overprint, represented by carbonate-rich pale mottled soils and calcrete horizons (Fig. 5D and 5E) and sharp to gradational boundaries.

Interpretation

The distribution of the lithofacies within the measured core sections allows to identify two main depositional sequences:

Mass-flow dominated alluvial fan sequence. This sequence exclusively consists of

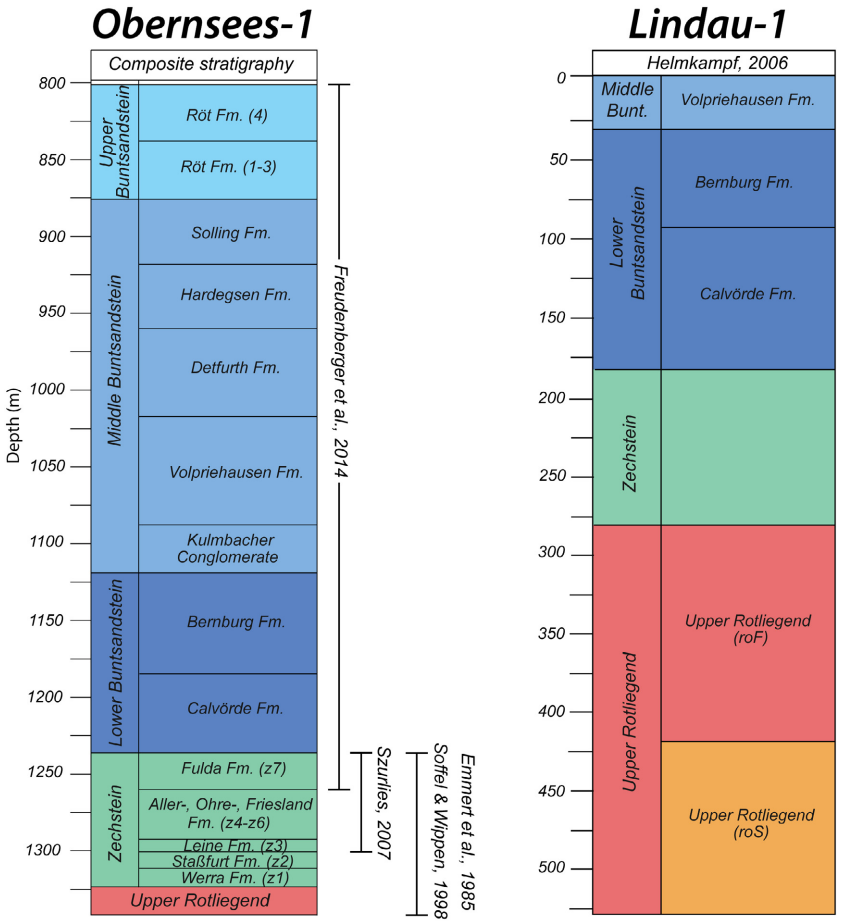

Fig. 4. Stratigraphic charts of the wells Obernsees-1 and Lindau-1. The composite stratigraphy of Obernsees-1 considers the most recent lithostratigraphic (Freudenberger *et al.*, 2014) and magnetostratigraphic (Szurlies, 2007) compilations of the Zechstein–Buntsandstein interval. The Rotliegend–Zechstein boundary is constrained via magnetostratigraphic and lithostratigraphic investigations (Emmert *et al.*, 1985; Soffel & Wippern, 1998). The stratigraphic framework of Lindau-1 is based on lithostratigraphy/gamma-ray schemes of Helmkampf (2006). The latter subdivided the Upper Rotliegend interval into roS and roF according to the dominant lithofacies association, respectively sandstone and fanglomerate. A specific colour code was chosen for each lithostratigraphic unit to simplify the visualization.

vertically stacked up breccia deposits (*Gmm* and *Gcm*). The absence of internal organization, random clast distribution, high matrix contents, and sharp boundaries of the matrix-supported beds points to non-confined medium to high viscosity clast-rich plastic debris flows and interleaved clast-poor mudflows (Bowman, 2019). Clast-supported deposits result from similar pseudoplastic, clast-richer debris flows, debris avalanche or grain flows (Miall, 2006). The higher clast to matrix ratio promotes kinetic filtering of smaller particles through larger ones during clast collision (Leeder, 1983). Sequences dominated by stacked-up breccia beds (Fig. 5H) typically occur in the proximal and medial settings of mass-flow dominated alluvial fan systems deposited under semiarid–arid climate with no or rare traction-current deposits (Fraser & Suttner, 1986; Calvache *et al.*, 1997).

Braided fluvial fan sequence. This sequence consists of massive breccia deposits (*Gmm* and *Gcm*) passing upward into cross-bedded (*Gtp*) and horizontal plane-bedded units (*Gh*) with associated massive claystone/siltstone beds (*Fm*) (Fig. 5I). Matrix-supported and clast-supported breccias result from the deposition of non-confined plastic to pseudoplastic clast-rich debris flows and clast-poor mudflows (Bowman, 2019). The presence of erosional boundaries and clast imbrication characterizing the cross-bedded deposits indicates a fluvial origin. The high clast angularity and the close association with breccia units suggest reworking of mass flow beds into high-energy fluvial gravel bars (Stanistreet & McCarthy, 1993). Horizontally bedded units indicate upper plane bed conditions related to the deposition of unconfined sheetfloods (Stollhofen & Stanistreet, 1994). Fine-grained beds overlying stratified conglomerates represent overbank elements accumulated in interfluve areas during flood events (Viseras & Fernández, 1994; Moscariello, 2018). Branching mottled soils testify to prolonged periods of fan inactivity or lobe/channel abandonment (Bowman, 2019). The association of erosionally

Table 1. Summary of the lithofacies identified within the Permian–Triassic sections subdivided according to the dominant grain-size and depositional process. See text for further explanations.

Facies code	Grain size	Bedding	Sedimentary structures	Top/base contacts	Depositional process	References
Gmm	Breccia, matrix-supported. Clasts from granule to cobble size, matrix from clay to very fine sand	Massive or faint flow lamination	Pedogenic overprint of unit top (palaeosols)	Sharp	Plastic debris flow (clast rich) and mud flows (clast poor)	Stanistreet & McCarthy (1993), Miall (2006)
Gmm[2]	Breccia, clasts from granule to pebble size	Weak normal grading trends, horizontally aligned clasts	Poikilotopic cement	Base: sharp Top: sharp, truncated	Subaqueous unconfined pseudoplastic debris flow with development of turbulent regime due to water admixing	Nemec & Steel (1988), Horton & Schmitt (1996)
Gcm	Breccia, clast-supported but matrix rich. Clasts from granule to pebble size	Massive or weak normal/reverse grain size grading	–	Sharp	Pseudoplastic clast-rich debris flow, debris avalanche or grain flow	Miall (2006)
Gh	Breccia/conglomerates, clast-supported. Clasts from granule to pebble size	Horizontal planar bedding to low-angle cross-bedding	–	Sharp	Upper flow regime plane bedding. Coarse sheetfloods, fluvial bar tops	Stollhofen & Stanistreet (1994), Calvache *et al.* (1997)
Gtp	Conglomerates, from granule to cobble size	Trough cross to planar cross-bedding (both high and low angle – <15°)	Clast imbrication, rip-up clasts	Sharp, erosional	Middle to upper part of lower flow regime. Minor channel fills. Gravel bedforms	Miall (1977)
Gm	Conglomerate, from granule to pebble size	Massive or crude horizontal stratification	Clast imbrication, rip-up clasts	Base: erosional, gradational Top: sharp	Middle to upper part of lower flow regime. Channel gravel bars and channel lags	Miall (1977)
Stp	Sandstones, fine to very coarse	Trough cross to planar cross-bedding (both high and low angle – <15°). Highly variable foreset dips	Rip-up clasts, mud drapes, gravel lags	Base: erosional, sharp, gradational Top: sharp, truncated, gradational	Upper part of lower flow regime. 3D or 2D dune-scale bedforms within the fluvial bed (longitudinal, transverse bars). Lateral point bar migration	George & Berry (1993), Miall (2006), Stanistreet & Stollhofen (2002)

Table 1. (continued)

Facies code	Grain size	Bedding	Sedimentary structures	Top/base contacts	Depositional process	References
Stb	Sandstone, medium to coarse	Trough cross-bedding, bimodal distribution of fine and medium to coarse sand layers	–	Sharp, base non-erosional	Grain fall and grain flow processes on lee flank of aeolian dunes	Clemmensen & Abrahmsen, 1983)
Sh	Sandstone, fine to coarse	Horizontal planar bedding	Bioturbation, calcrete	Sharp	Upper flow regime plane bedding. Fluvial bar tops	Miall (2006), Minervini *et al.* (2011)
Shr	Sandstones, fine to medium	Pinstripe lamination in sand by thin silt layers	Bioturbation and thin lenses of coarse sand	Sharp	Migration of wind ripples on moist sand/mud-flat. Coarser sand lenses due to aeolian winnowing	Fryberger & Schenk (1988), Henares *et al.* (2014)
Smc	Carbonate cemented sandstones, fine to coarse	Massive, remnant horizontal to low-angle (<15°) planar cross-bedding	Poikilotopic cement, thin dark horizontal to inclined laminae (<3 cm thick)	Base: sharp, erosional Top: sharp	Low-density turbulent flow, hyperpycnal flows	Bourquin *et al.* (1998), Mulder *et al.* (2003), García-García *et al.* (2011)
Sm	Sandstones, very fine to very coarse	Massive or faint lamination	Rip-up clasts, carbonate precipitation, palaeosols, rare convolution	Base: erosional, gradational Top: sharp, truncated, gradational	Lower or upper flow regime. Sandy bedforms	Miall (2006)
Sm^{2}	Sandstones, fine to coarse	Massive, some matrix content, grain with aeolian texture	–	Sharp	Mud admixing in the upper part of the lower flow regime during flood episodes. Hyperconcentrated streams	Svendsen *et al.* (2003)
Sm^{3}	Sandstones, very fine to medium	Massive, disrupted bedding with remnants of wavy lamination	Irregular sandy lenses, mud drapes, layerwise carbonate nodules, anhydrite/gypsum pseudomorphs, intraformational mud-clasts	Sharp	Sand trapping process by salt crust and subsequent burial dissolution	Clemmensen (1985), Goodall *et al.* (2000)
Sm^{4}	Sandstones, very fine to fine	Massive, rare faint bedding	Intense bioturbation, carbonate cementation, mud drapes, oolitic laminae	Sharp	Subaquatic deposition in a low energy environment with occasional influx from shoreface	Warren (2006), Słowakiewicz *et al.* (2013)

Table 1. (continued)

Facies code	Grain size	Bedding	Sedimentary structures	Top/base contacts	Depositional process	References
Fl	Siltstones to fine sandstones	Ripple to plane-lamination	Flaser lamination, bioturbation	Sharp	Lower flow regime. Deposition from suspension load. Overbank levées, channel abandonment, waning flood, crevasse splay	Miall (2006), Viseras *et al.* (2018)
Fm	Mudstone to very fine sandstone	Massive	Bioturbation, desiccation cracks, pedogenic overprint, root prints	Sharp, gradational	Lower flow regime. Deposition from suspension load. Overbank, channel abandonment, waning flood	MIall (2006), Viseras *et al.* (2018)
Fm^2	Claystone to siltstone	Massive, rare faint bedding	Bioturbation, primary carbonate and minor anhydrite nodules, cluster and layers of gypsum crystals and pseudomorphs	Sharp	Deposition under the water table in low energy environment	Clemmensen (1985), Warren (2006)

based, cross-bedded gravel units with sheetflood and mass flow beds (Fig. 5I) points to deposition in the medial part of a braided fluvial fan system (Stanistreet & McCarthy, 1993; Moscariello, 2018).

Interbedded cemented breccia and sandstones: fan-delta deposits

This lithofacies association includes poorly sorted massive whitish breccia (*Gmm*^{2}) and sandstone beds (*Smc*), both displaying intense carbonate cementation (Fig. 5J). Massive gravel deposits exhibit a random distribution of angular to sub-angular granule and pebble-sized clasts, rare and faintly developed small-scale (<0.1 m) normal grading trends and occasional horizontal alignment of pebbles (Fig. 5F and 5G). Thicknesses range between 0.3 to 1.2 m. Bed boundaries are sharp and/or scoured at the bases of sandstone units (*Smc*), which are massive or display faint low-angle cross-bedding (<15°) to horizontal bedding (Fig. 5G). Thicknesses of the sandstone beds range between 0.3 to 0.6 m. Thin dark horizontal to inclined mud laminae (<3 cm thick) mark single set-tops.

Interpretation

Thin dark mud laminae represent fallout from suspension, indicating a temporary restoration of low-energy settings and represent the upper portion of subaqueous channel infills or lobe elements (Tan *et al.*, 2018). The sharp boundaries and the random clast distribution of the breccia deposits indicate laminar flow conditions (Horton & Schmitt, 1996) associated with the deposition of pseudoplastic debris flows or mudflows. Conversely, normal grading trends and horizontal pebble alignment suggest occasional development of turbulent regimes (Nemec & Steel, 1988; Horton & Schmitt, 1996). These features and the association with suspension-fallout deposits point to subaqueous depositional settings with admixture of water favouring increased turbulence, decreased matrix strength and dispersive pressure (Horton & Schmitt, 1996; García-García *et al.*, 2011). The poikilotopic character of the carbonate cement strengthens this interpretation, indicating a subaqueous formation in a hypersaline setting (Warren, 2000). The massive to planar low-angle cross-beddings, erosive bases and the association with breccia beds are all diagnostic of deposition under a low-density turbulent regime commonly associated with hyperpycnal flows (Fernández *et al.*, 1993; Bourquin *et al.*,

Table 2. Summary of the lithofacies associations and corresponding depositional environments.

Facies Association	Sequence type	Depositional environment	Reference
Breccia beds: Mass flow/Fluvial fan deposits	Stacked *Gmm* and *Gcm*	Proximal to medial portion of gravity-flow dominated alluvial fan	Fraser & Suttner (1986), Calvache *et al.* (1997), Bowman (2019)
Breccia beds: Mass flow/Fluvial fan deposits	*Gmm, Gcm, Gtp, Gh* and *Fm*	Medial area of braided fluvial fan system developed through sediment accumulation by distributive braided channels and non-channelized flood	Stanistreet & McCarthy (1993), Viseras & Fernández (1994), Moscariello (2018)
Interbedded cemented breccia and sandstone: Fan-delta deposits	*Gmm*^{2} and *Smc*	Proximal fan-delta settings, dominated by gravity-flows and low-density turbulent flows or hyperpycnal flows	Fernández *et al.* (1993), Horton & Schmitt (1996), García-García *et al.* (2011)
Conglomerates to fine: Fluvial deposits	*Gtp*, *Gm*, *Stp,* rare *Gh* and *Gmm*	Gravel dominated braided fluvial settings with perennial characters and sporadic progradation of single lobe fan	Miall (2006), Allen *et al.* (2013)
Conglomerates to fine: Fluvial deposits	*Stp, Sh, Sm* and *Fm*	Intermittent channelized fluvial deposition and unconfined flash flood	Frostick & Reid (1977), Lowe & Arnott (2016)
Conglomerates to fine: Fluvial deposits	*Stp, Sm,* frequent *Fl, Fm* and occasional basal *Gtp* and *Gm*	Higher-sinuosity channel infill attributed to meandering depositional settings with abundant floodplain elements	Miall (2006), Viseras *et al.* (2006), Donselaar & Overeem (2008)
Bimodal sandstones: Mixed fluvio-aeolian deposits	*Stb* alternated to *Stp* and *Sm*^{2}, and isolated *Shr*	Aeolian dune mixed ephemeral fluvial deposition and hyperconcentrated flow in the interdune area. Aeolian sandflat	Clemmensen & Abrahmsen (1983), Stanistreet & Stollhofen (2002), Henares *et al.* (2014)
Sandstones to mudstone: Sabkha to shallow marine deposits	*Sm*^{3}, *Sm*^{4}, *Fm*^{2} and *Fl*	*S*iliciclastic-dominated dry coastal sabkha to shallow-marine environment and hypersaline restricted lagoon	Clemmensen (1985), Briere (2000), Paul (2006), Warren (2006), Słowakiewicz *et al.* (2013)

1998; Mulder *et al.*, 2003; Soria *et al.*, 2003; García-García *et al.*, 2011). Accordingly, the described association (Fig. 5J) defines proximal fan-delta settings produced by the progradation of alluvial fan aprons into a water body (Horton & Schmitt, 1996).

Conglomerates to fines: fluvial deposits

This association consists of poorly to moderately sorted reddish to whitish conglomerate/pebbly-sandstones (*Gtp, Gh* and *Gm*), sandstones (*Stp*, *Sh* and *Sm*), minor dark red to greenish clayey-silty layers (*Fl* and *Fm*) and rare breccia interbeds (*Gmm*). Conglomerates dominantly consist of subrounded to rounded clasts ranging between granule and cobble size. They are either massive with no or crude stratification (lithofacies *Gm*) or display trough or planar cross-bedding (lithofacies *Gtp*) (Fig. 6A and 6B). Bed boundaries are sharp, locally erosive, and commonly associated with clast imbrication. Thicknesses range between 0.2 to 2.0 m. Sharp-bounded conglomerates subordinately exhibit horizontal bedding (lithofacies *Gh*) with thicknesses between 0.2 to 0.6 m (Fig. 6A and 6B). Breccia interlayers consist of thin (0.2 to 0.5 m thick) and sharp-bounded matrix-supported gravel beds (lithofacies *Gmm*) (Fig. 6B) carrying pebble-sized clasts floating in a Fe-rich clay-silty matrix. Trough and planar cross-bedded deposits (lithofacies *Stp*) characterize fine to very coarse sandstones (Fig. 6B to 6G), locally recording highly variable foreset dips within a set (Fig. 6H). Basal boundaries vary from sharp, transitional to often scoured and floored by gravel-size intraformational rip-up clasts. Bed thicknesses vary from a few centimetres to 6 m. Some sandstones

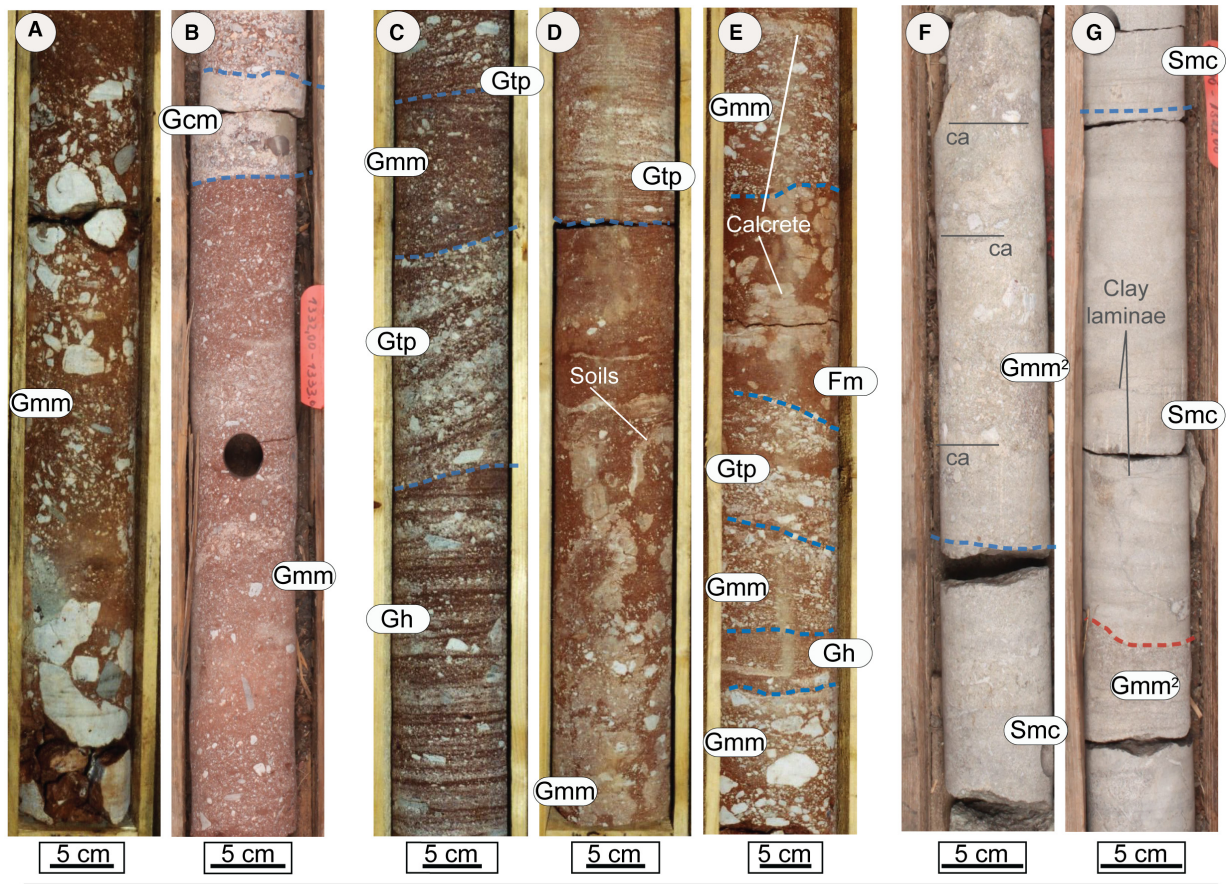

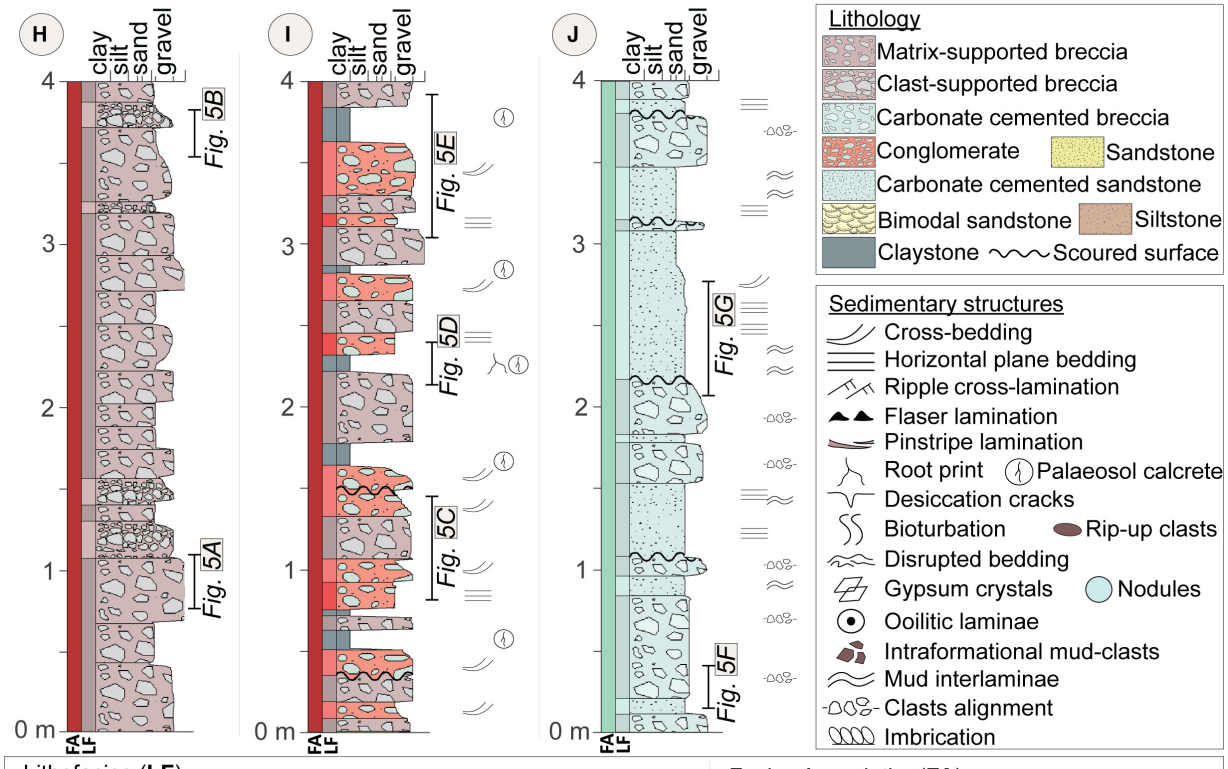

Fig. 5. Examples of gravel dominated lithofacies. Blue dashed line: set boundary; red dashed line: scoured surface. (A) Cobble to pebble size clasts floating in a fine matrix (*Gmm*). Notice the slight fining-upward sequence overlain by coarser pebble deposits, interpreted as a set of stacked flow units. (B) *Gmm* lithofacies overlain by clast-supported *Gcm* unit. Notice the normal grain-size trend within *Gcm*. (C) Upper flow regime plane-bedded gravel bed (*Gh*) evolving into high-angle cross-bedded conglomerate (*Gtp*). Upward, a mass-flow unit (*Gmm*) is overlain by *Gtp*. (D) *Gmm* deposits displaying palaeosol features (rhizoliths, mottling, carbonate concretions) are overlain by poorly sorted, low-angle plane to cross-bedded granule conglomerates (*Gtp*). (E) Stacked *Gmm* and *Gh* interpreted as debris flow and sheetflood deposits evolving into cross-bedded fluvial conglomerate (*Gtp*) and overlain by massive and pedogenically overprinted mudstone (*Fm*). A new depositional cycle initiates with the overlain breccia element. (F) and (G) Stacked carbonate cemented breccia units (*Gmm*^{2}) and massive sandstones (*Smc*), locally displaying erosive base. Notice the horizontal clast alignment (ca) within the *Gmm*^{2}, and the thin black mud laminae and faint horizontal bedding in *Smc*. (H) Schematic litholog of mass flow dominated alluvial fan sequences. (I) Schematic litholog of braided fluvial fan sequences. (J) Schematic litholog of fan-delta sequences.

alternatively display either horizontal plane-lamination (lithofacies *Sh*) or are massive with rarely preserved bedding remnants (lithofacies *Sm*), convolutions, bioturbations and basal rip-up clasts (Fig. 6C, 6D and 6E). Thicknesses range between 0.2 to 2.3 m. Fine-grained deposits either consist of thin siltstones to very fine sandstones displaying unidirectional ripple cross-lamination and flaser bedding (*Fl*) or massive clay/silt layers (*Fm*). The latter often display bioturbations, locally root prints and V-shape, occasionally sandy-filled and deformed desiccation cracks (Fig. 6D, 6F and 6G). Beds boundaries are sharp, and thicknesses range between 0.06 to 0.5 m.

Interpretation

Despite that there is insufficient evidence for univocally discriminating the fluvial architecture (Swan *et al.*, 2018), the lithofacies distribution defines three endmember sequences indicative of different depositional styles:

Braided sequence. This sequence consists dominantly of stacked cross-bedded or massive conglomerates (*Gtp* and *Gm*), associated with minor horizontally bedded gravel deposits (*Gh*) and rare breccia (*Gmm*), or grading upward into thin sandy macroforms (*Stp*) (Fig. 6I). Floodplain elements are scarce, forming a maximum 6% of the sequence thickness. There is almost no presence of overbank reworking, for example as testified to by the absence of soft clasts (Henares *et al.*, 2016a). All this suggests bedload dominated streams. Gravel units are relatively thin with poorly scoured erosional bases. Such an association may reflect the infill of shallow braided channels with stacked-up cross-bedded conglomerates occasionally truncated by minor erosional surfaces resulting from the migration of channel bars deposited under high-energy flow conditions (Miall, 1977; Viseras & Fernández, 1994). Occasional sandstones at the top of weak fining-upward cycles may represent the upper portions of the migrating gravel bars (Miall, 1985) deposited under waning flow conditions (Fig. 6A). Rare plane-bedded gravel beds reflect the achievement of transcritical to supercritical flow and result from deposition under shallow water conditions, which are common in fluvial bar-tops and coarse unconfined sheetfloods (Stollhofen & Stanistreet, 1994; Calvache *et al.*, 1997). The dominance of cross-bedded deposits over plane-parallel bedding indicates a relatively continuous discharge regime. Furthermore, there is no evidence of long-term subaerial exposure, such as soil development. These criteria all imply a perennial character of the fluvial system (Allen *et al.*, 2013; Ielpi & Ghinassi, 2015; Henares *et al.*, 2020). The sporadic occurrence of interbedded non-confined plastic debris-flow deposits may indicate local progradation of single fan lobes (Miall, 2006).

Intermittent channelized and ephemeral flash-flood sequence. These units dominantly consist of stacked weakly developed fining-upward cycles where plane-laminated and massive beds (*Sh* and *Sm*) overlie basal-scoured cross-bedded deposits (*Stp*) and evolve upsection into massive mudstones (*Fm*) (Fig. 6J). Basal cross-bedded sandstones result from the migration and superimposition of 2D (planar cross-bedded) and 3D (trough cross-bedded) longitudinal and transverse bars, sidebars, point-bar and sand waves (Miall, 2014; Swan *et al.*, 2018). In contrast, plane horizontal-bedding records prevailing upper flow regime conditions of temporary

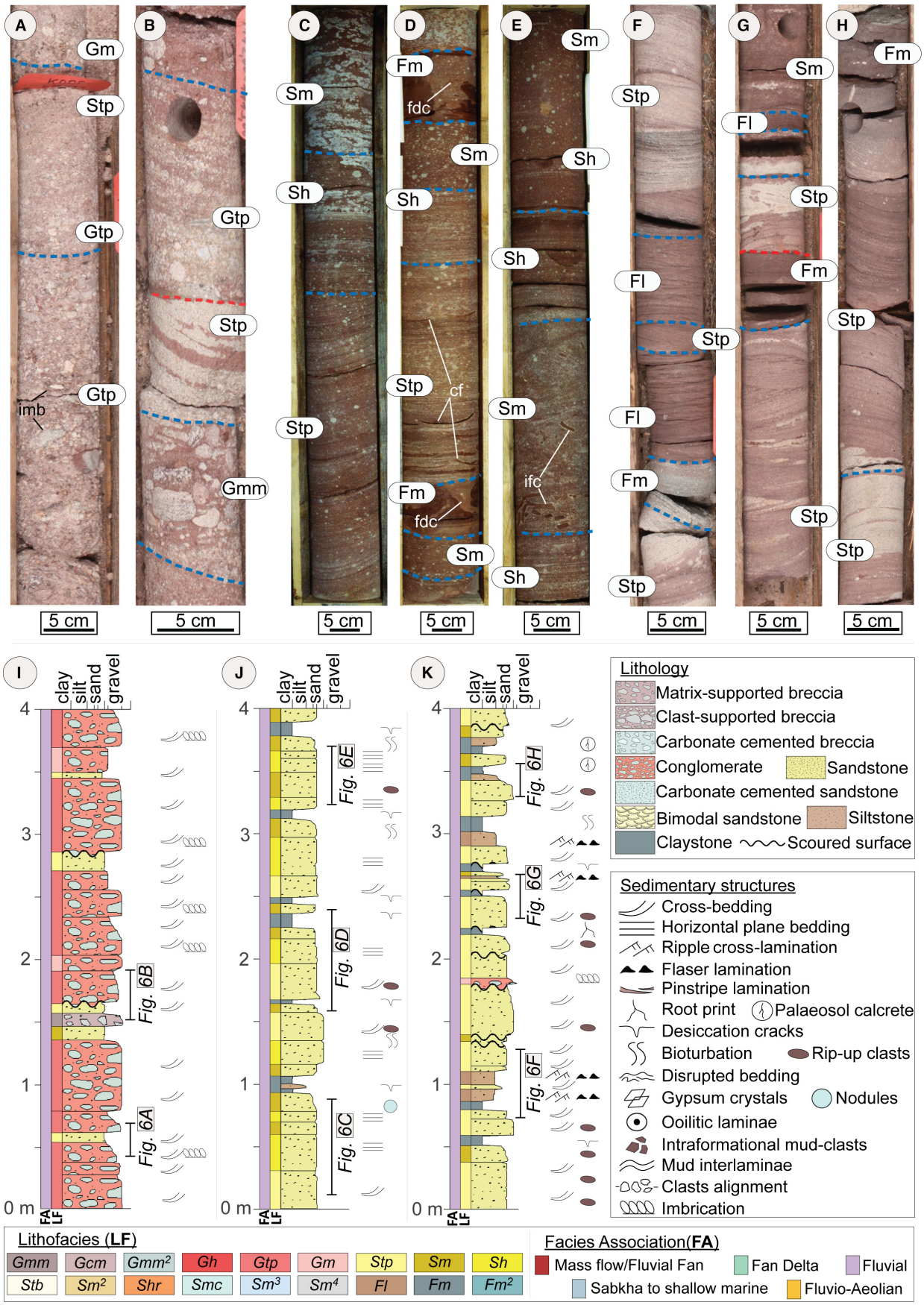

Fig. 6. Examples of fluvial deposits. Blue dashed line: set boundary; red dashed line: scoured surface. (A) Basal trough cross-bedded conglomerates (*Gtp*) exhibiting imbrication (imb) of rounded pebble to granule-size grains upward evolving into cross-bedded sandstone (*Stp*). A massive conglomeratic layer (*Gm*) marks the onset of a new flood cycle. (B) Thin breccia unit (*Gmm*) interbedded to stacked cross-bedded sandstones. Cross-bedded conglomerates with normal grain-size trend erosionally overlay the sandstones. (C) Medium to fine cross-bedded sandstones (*Stp*) grading into horizontal plane-laminated (*Sh*) and massive *(Sm*) deposits affected by groundwater carbonate precipitation (white colour). (D) Massive (*Sm*) and normal grading cross-bedded (*Stp*) sandstones, separated by thin mudstone interval (*Fm*). V-shaped sandy filled desiccation cracks (fdc) in *Fm* with deformation caused by differential compaction. Concave up clay flakes (cf) occur within *Stp*. (E) Plane laminated medium sandstone (*Sh*), overlaid by an intensely convoluted unit containing abundant intraformational clay clasts (ifc), and upward evolving into stacked *Sh* and *Sm* elements. (F) Medium grained cross-bedded sandstones grading into massive mudstone (*Fm*) and ripple laminated siltstone (*Fl*). *Stp* deposits mark the beginning of a superimposed fining-upward cycle. (G) Stacked-up fining-upward cycles displaying basal *Stp* beds, with scoured base and clay clasts, evolving into massive or ripple-laminated mudstone units. (H) Cross-bedded sandstones (*Stp*) with upward decrease of the foreset steepness and fining upward tendency. The massive mudstone at the top display carbonate concretions. A thin gravel lag element separates to stacked sequences. (I) Schematic litholog of gravel-dominated braided fluvial sequences. (J) Schematic litholog of sandstone-dominated intermittent channelized and ephemeral flash-flood fluvial sequences. (K) Schematic litholog of high-sinuosity fluvial sequences.

unconfined sheetfloods (after Minervini *et al.*, 2011). The upward transition from cross-stratified sandstones to horizontal plane-bedded and massive deposits (Fig. 6J) reflects the sedimentary evolution from initially rather confined channels to unconfined sheetflood deposition during flood peaks (Frostick & Reid, 1977; Lowe & Arnott, 2016). Abundant intraformational soft clasts flooring scoured surfaces reflect cut-wall erosion of floodplain elements (Fig. 6E) (Henares *et al.*, 2016b). The common occurrence of desiccation features points to frequent periods of subaerial exposure (Allen *et al.*, 2013). Deformed sand-filled desiccation cracks (Fig. 6D) record differential compaction after the rapid deposition of flash flood sand units (Rieke *et al.*, 1974). In summary, these units record a change of the dominant flow regime and a transition from overwhelming perennial/intermittent to ephemeral streams.

High-sinuosity fluvial sequence. The deposits are organized within stacked fining-upward cycles (0.8 to 6.0 m thick), where basal-scoured cross-bedded sandstones (*Stp*) – occasionally overlying thin gravel units (*Gtp* and *Gm*) – grade upward into rather thick laminated or massive mudstones units (*Fl* and *Fm*) (Fig. 6K). Obvious basal scours overlain by thin gravel lenses, the highly variable cross-bed dips (Fig. 6H) and pronounced fining-upward trends point to lateral accretion of side/point-bar elements of mixed load rivers with increased sinuosity (Miall, 1985; Yeste *et al.*, 2020). Fines form up to 30% of the sequence thicknesses, reflecting considerable suspended river-load. Ripple-laminated and massive mudstones capping the sequences reflect falling stages and settling of suspended sediment load under lowermost to stagnant flow regimes in floodplain or abandoned channel settings (Olsen, 1987; Viseras *et al.*, 2018). Common root prints and desiccation features are indicative of subaerial exposure and pedogenetic overprint of exposed floodplains (Walker, 1984; Miall, 2006; Galloway & Hobday, 2012). Thin ripple-laminated sandstones interbedded with massive mudstones may represent crevasse splay and rare levée deposits (Gulliford *et al.*, 2017; Yeste *et al.*, 2020). Conglomeratic beds occasionally occurring at the bottom of the fining-upward cycles may represent either remnant higher energy gravel bedforms or channel lag deposits (Miall, 2006). The vertical succession here matches the fluvial records generated by the lateral accretion of point-bar elements and widespread floodplain deposits (Viseras *et al.*, 2006; Donselaar & Overeem, 2008). Accordingly, the described endmember sequence is herein attributed to the deposition of higher sinuosity, mixed load dominated fluvial settings, typical of a meandering regime.

Bimodal Sandstones: mixed fluvio-aeolian deposits

This lithofacies association is dominated by well-sorted whitish sandstones exhibiting either grain size bimodality (*Stb*) or unimodality (*Spt* and *Sm*^{2}), and characterized by well-rounded

grains and a complete lack of mica and detrital matrix. Bimodal sandstones consist of 2 to 4 mm thick medium to coarse-grained sand layers alternating with 1 to 2 mm thick fine sand laminae of trough cross-bedded (lithofacies *Stb*) and non-erosive based units (Fig. 7A and 7B). Thicknesses range between 0.3 to 0.8 m. Unimodal sandstones mostly exhibit trough cross-bedding (lithofacies *Stp*), sharp erosive bases associated with basal rip-up clasts (Fig. 7B) and thicknesses between 0.3 to 0.8 m. Cross-bedded sandstones stack-up into vertical aggrading sets alternating with massive sand beds displaying unimodal, well-sorted grain-size distribution and occasional clay laminae (lithofacies Sm^2). A further lithofacies of this association consists of sharp-bounded whitish to reddish fine to medium sandstones displaying plane-bedding, rarely low-angle cross-bedding with pinstripe-laminated silt and rare flat lenses of coarse sand (lithofacies *Shr*) (Fig. 7C). Thicknesses range between 0.4 to 0.8 m. Occasionally bioturbation marks bed tops.

Interpretation

Sorting, grain roundness, and the absence of matrix and mica, all indicate high sand maturity, which is common in aeolian dominated environments. Grain-size bimodality reflects the alternation of finer grain fall (ballistic fallout) and coarser grain flow (avalanche) processes at lee slopes of aeolian dunes with kinetic sieving eventually causing inverse gradation (Clemmensen & Abrahmsen, 1983). Both the textural composition and the presence of scoured bases and mud clasts of unimodal cross-bedded sandstones imply short-term erosion, reworking and redeposition of aeolian sands and interdune deposits by ephemeral streams (George & Berry, 1993; Stanistreet & Stollhofen, 2002). Sediment loads of such streams may rise considerably during flood cycles, with the admixing of mud favouring overloaded streams transitional to hyper-concentrated flows (Svendsen *et al.*, 2003). The latter might explain the observed combination of trough cross-bedded to massive sandstones deposited in interdune areas or outside a dunefield (Fig. 7I). Pinstripe-laminated deposits reflect the alternating deposition of aeolian transported grains from saltation (sandy layers) and suspension fallout (silt laminae) (Fryberger & Schenk, 1988; Henares *et al.*, 2014). These aeolian sheets preferentially accumulate on low relief damp sandflats and mudflats of interdune areas or in front of fan lobes/apron settings during periods of restricted aeolian sediment supply. Small lenses of coarse-grained sand are probably deflationary lag grains, whereas bioturbation indicates periods of non-deposition.

Sandstones to mudstones: sabkha to shallow marine deposits

This lithofacies association is dominated by fine to medium reddish to whitish sandstones and mudstones stacked up into aggrading sequences or occurring isolated and interbedded with the lithofacies of the previous associations. Sandstones usually display massive fabric and disrupted bedding, rarely preserving remnant wavy lamination, including thin mud drapes, irregular sand lenses and platy angular intra-formational mud-clasts (Sm^3) (Fig. 7D and 7E). Thicknesses range between 0.2 to 0.8 m. White carbonate nodules (4 to 12 mm) exhibiting displacive growth occur as both isolated (Fig. 7F) or as layer-wise coalesced clusters within the sandstones. Massive beds alternatively display faint lamination and intense carbonate cementation (Fig. 7G). Rare recrystallized ooids (<1 mm of

Fig. 7. Examples of aeolian and sabkha deposits. Blue dashed line: set boundary. (A) Trough cross-bedded sandstones showing bimodal distribution (bm) of medium to coarse and fine sand layers. (B) Trough cross-bedded deposits (*Spt*), containing rip-up clasts (ruc), upward evolving into massive (Sm^2) and cross-bedded bimodal sandstones (*Sbt*). The sequence as a whole reflects a transition from reworked aeolian sands to massive, matrix bearing aeolian beds deposited by hyperconcentrated flows in interdune areas, capped by aeolian dunes deposits. (C) Typical pinstripe-lamination (*Shr*), consisting of thin silt laminae in plane-bedded, well-sorted, fine to medium sandstones. (D) Massive medium sandstone bed marked by wispy or disrupted 'lamination' and mottling due to redox reactions. (E) Massive sandstone beds with pervasive cementation (Sm^3), containing angular intraformational clay-clasts (ifc) and a thin Fm^2 layer interbed. (F) Massive very fine sandstone (Sm^3) grading into Fm^2 containing carbonate nodules. (G) Intensively cemented sandstone displaying frequent clay laminae and faint lamination (Sm^4) grading upward into ripple laminated siltstone (*Fl*). (H) Thick interval of massive clay/siltstones containing clusters of euhedral lenticular gypsum (gyp) crystals. (I) Schematic litholog of fluvio-aeolian sequences. (J) Schematic litholog of sabkha to shallow marine sequences.

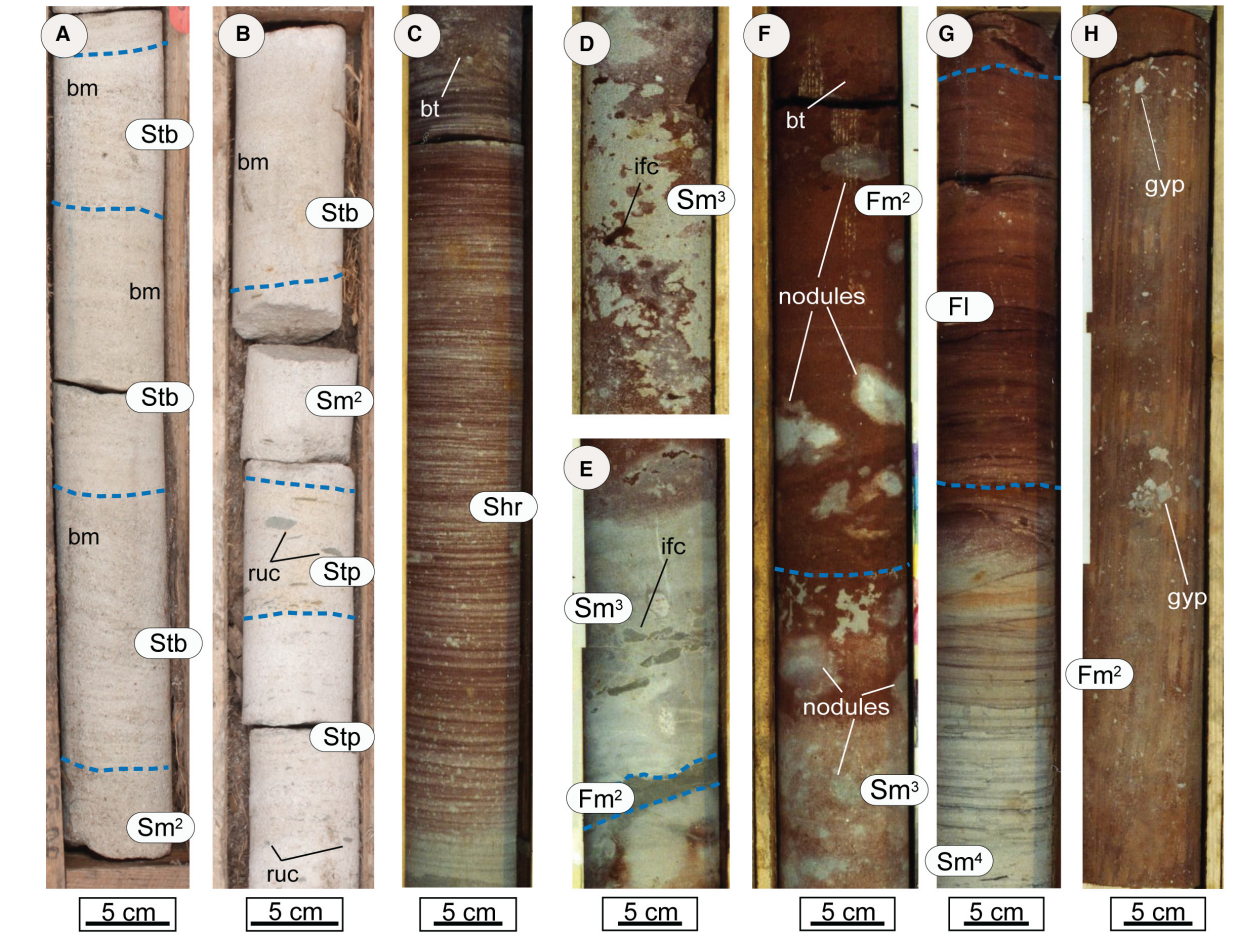

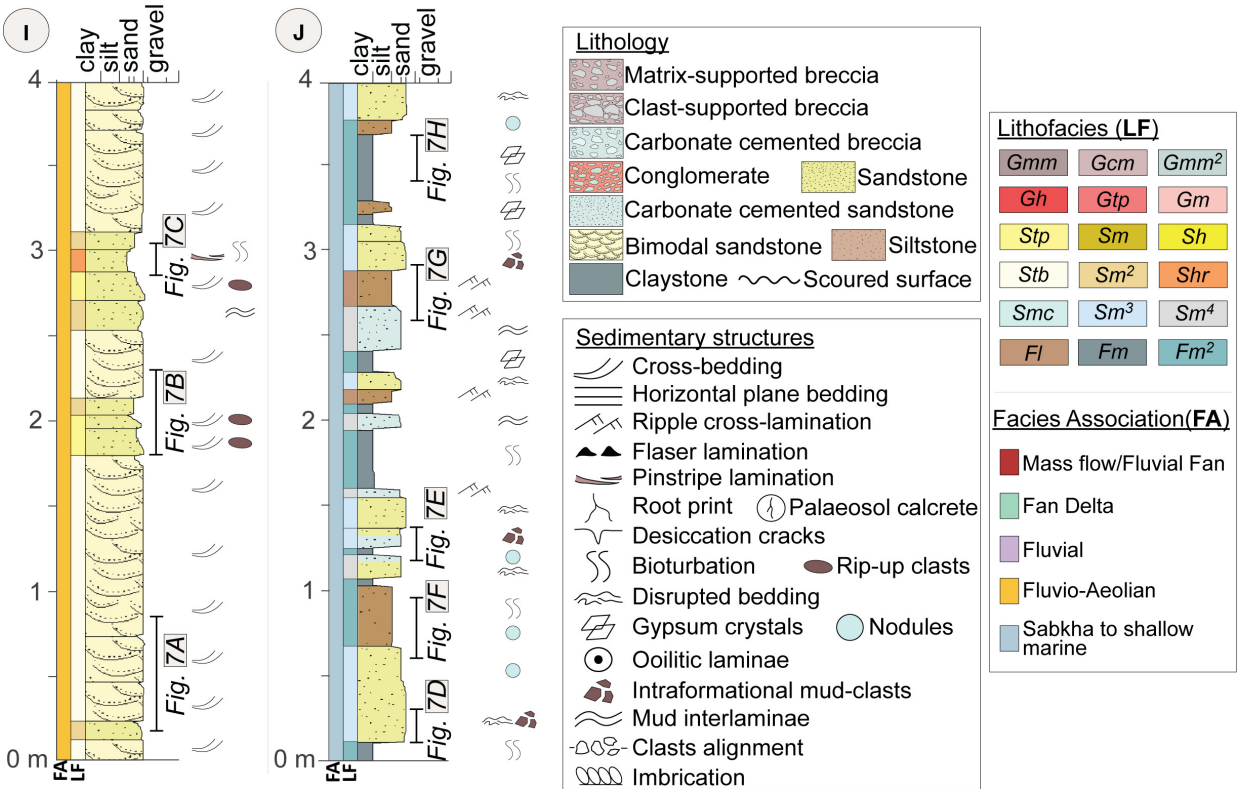

diameter) occur in laminae and mixed with the siliciclastic grains (*Sm*[4]). Mudstones dominantly consist of massive and often bioturbated clay–silty deposits (lithofacies *Fm*[2]) with highly variable thicknesses between 0.8 to 6.0 m and rare interbeds of ripple to plane-laminated very fine sandstone/siltstone (lithofacies *Fl*). Massive beds locally exhibit primarily gypsum and less abundant anhydrite nodules or random and strata bound lenticular clusters of euhedral gypsum pseudomorphs (Fig. 7F and 7H).

Interpretation

Displacive carbonate nodules and disrupted bedding in massive sandstones reflect multiple swelling and shrinking phases during water contact and drying out associated with mineral growth and dissolution. Remnant wavy lamination suggests that sand transported by saltation was trapped by damp salt-encrusted muddy surfaces (Smoot & Castens-Seidell, 1994; Goodall *et al.*, 2000). Carbonate nodules are indicative of chemical precipitation from groundwater or subaerial pedogenetic processes under arid climate conditions (Mack *et al.*, 1993; Tabor *et al.*, 2017). In contrast, thick mudstone intervals lacking desiccation features and showing intense bioturbation point to deposition in low-energy subaqueous environments (Antrett, 2013). Thus, the described association preserves evidence of both subaqueous and subaerial deposition within a siliciclastic-dominated dry coastal sabkha to shallow-marine environment (Fig. 7J) (Clemmensen, 1985; Briere, 2000). Evidence for gypsum crystals and carbonate cementation support this interpretation (Eugster, 1980). Modern analogues are well-described from the Bristol Dry Lake of the Mojave Desert in south-eastern California (Handford, 1982) and from the Middle East (Amiel & Friedman, 1971). Bioturbations and mud-drapes associated with oolitic laminae (Paul, 2006) may record deposition in hypersaline, more restricted lagoon settings, occasionally receiving storm-related sand influx from the nearby-shoreface (Warren, 2006; Słowakiewicz *et al.*, 2013).

CHANGES IN THE DEPOSITIONAL SETTINGS ACROSS THE PERMIAN–TRIASSIC TRANSITION

Detailed sedimentological core-logging and facies interpretations allow to constrain the environmental evolution from the successions recorded in Obernsees-1 and Lindau-1. Extensive sandflats occur in the Rotliegend (roS) of Lindau-1 (Fig. 8), resulting from the deposition of distal-fan derived ephemeral sheetfloods periodically replacing more channelized stream systems. Braided fluvial fans form the Rotliegend (roF), reflecting fan progradation over previously established sandflat environments and resulting in an overall coarsening-upward tendency across the entire Rotliegend. The occasional presence of interbedded sandstones and massive clay deposits displaying euhedral gypsum crystals (Fig. 8) points to some fluvial fan interactions with coastal sabkha elements during short-term sabkha flooding. Conversely, the Upper Rotliegend sequence overlying the basement in Obernsees-1 (Fig. 9) consists of stacked breccias deposited in mass flow-dominated alluvial fan settings.

The Zechstein records remarkable changes in the depositional conditions. Fan-deltas develop in Obernsees-1, replacing the underlying Rotliegend subaerial alluvial fans. Sandflat beds, displaying ephemeral fluvial transport, and thick massive mudstone sequences recording shallow-marine/coastal sabkha conditions occur above, delineating an overall fining-upward tendency resulting from base-level rise (Fig. 9). The remaining Zechstein (*Aller – Fulda Formation*) of Obernsees-1 records a coarsening-upward trend accompanied by the restoration of fluvial settings. Particularly the establishment of fine-grained sandstones displaying pronounced fining-upward cycles, commonly scoured at the bottom, and associated with abundant floodplain elements is indicative of a high sinuosity meandering fluvial style. The Rotliegend–Zechstein transition occurs abruptly in Lindau-1, pinpointed in the core log by the occurrence of ooid-layers formed in a restricted lagoon setting (Paul, 2006) (Fig. 8). Interdigitated aeolian/fluvial sandflat and sabkha depositional elements form the remaining Zechstein. The succession mainly developed in siliciclastic coastal environments where sedimentation is influenced by frequent fluctuations of the sea-level. Overall, the Zechstein of Lindau-1 displays a weak coarsening-upward tendency with a relatively increased abundance of fluvial and floodplain beds in the uppermost portion.

The Buntsandstein records the return to purely continental deposition, building up hundred metres thick sedimentary sequences associated with changes in fluvial styles and the establishment of more perennial flow regimes (Figs 8 and 9). Pinpointing the exact positions

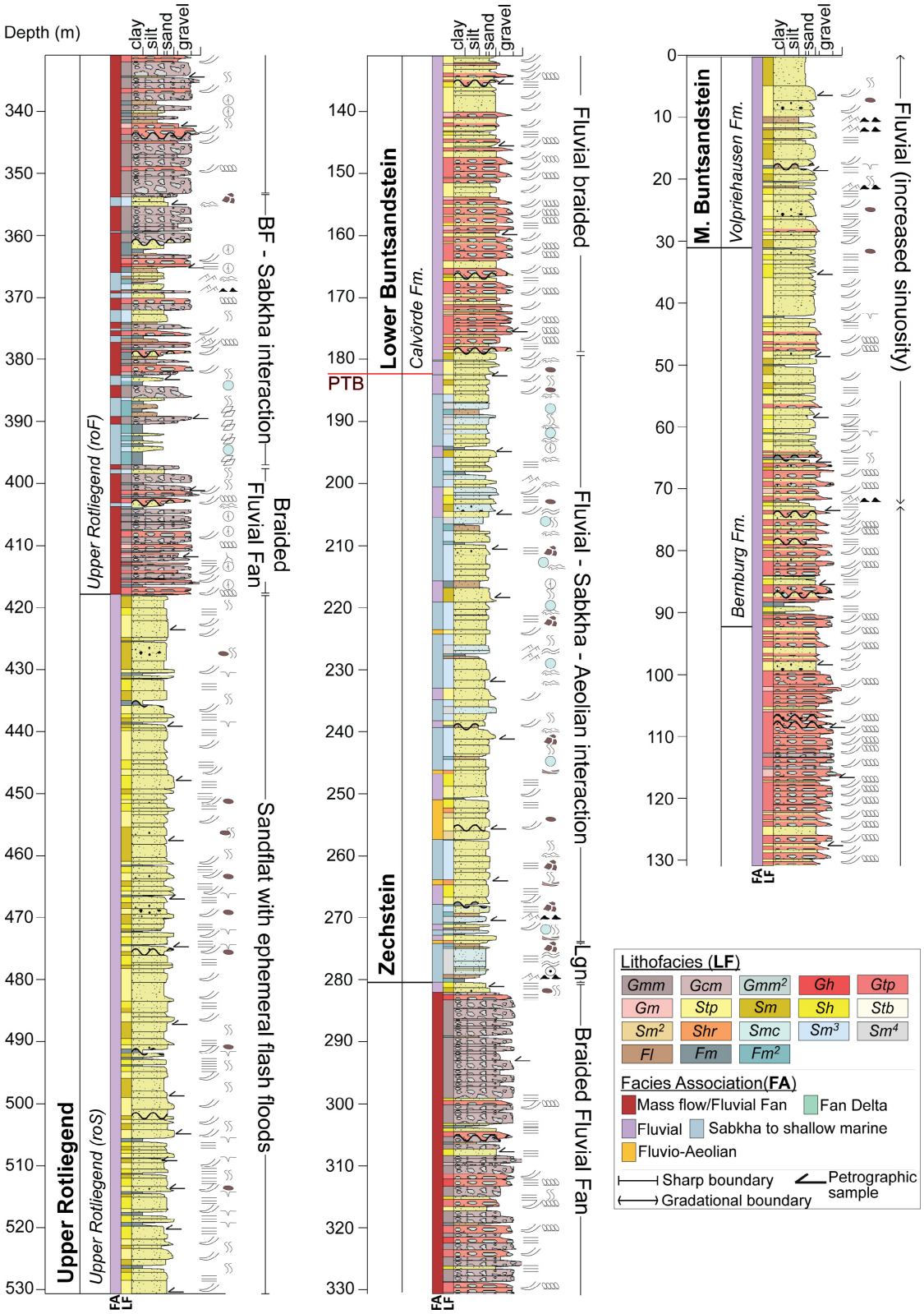

Fig. 8. Sedimentological evolution and interpreted depositional environment across the Rotliegend–Buntsandstein sequence of the well Lindau-1. BF, Braided fluvial Fan; Lgn, Lagoon settings. Detailed legend lithology and sedimentary structures on Figs 5 to 7.

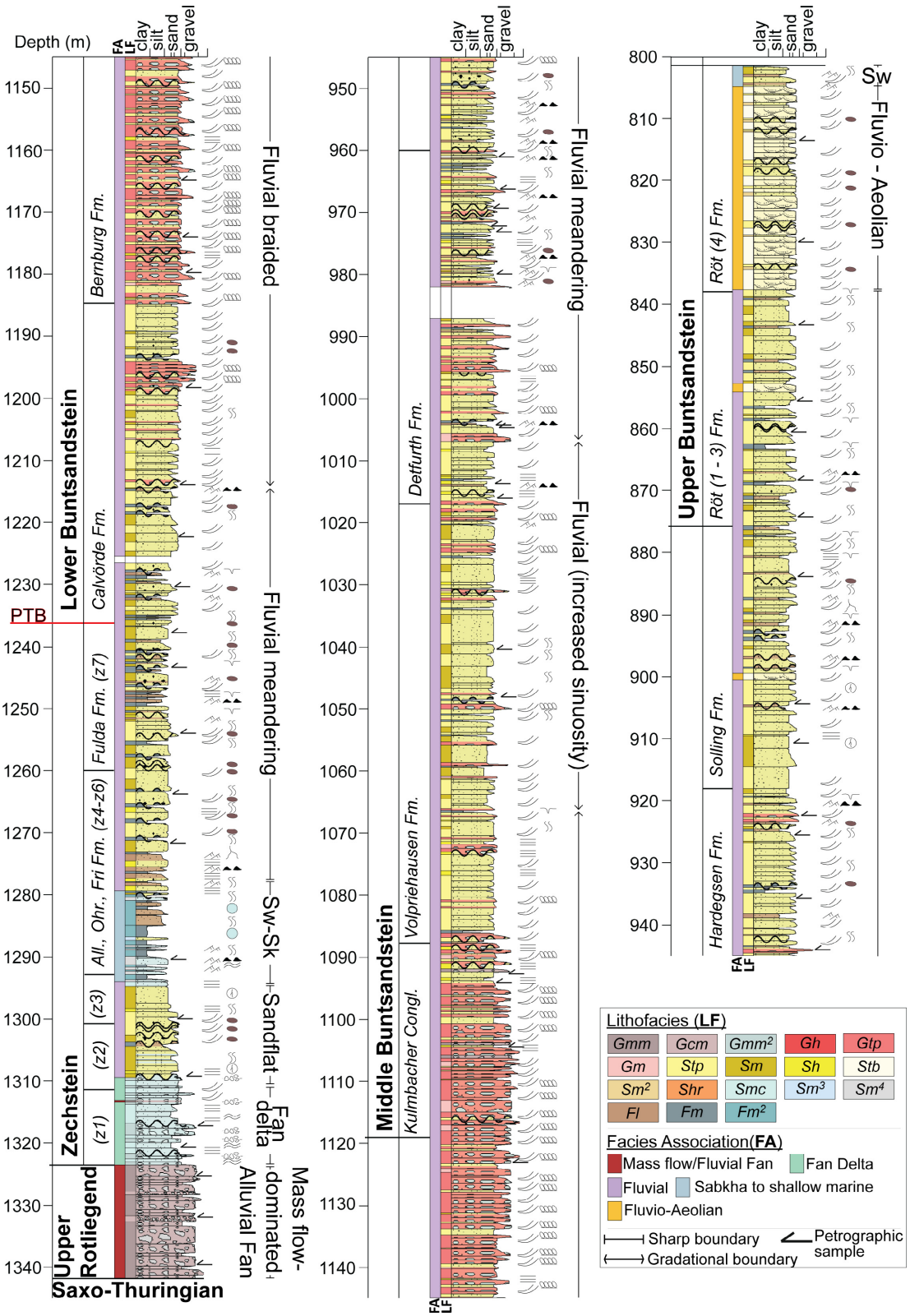

Fig. 9. Sedimentological evolution and interpreted depositional environment across the Rotliegend–Buntsandstein sequence of the well Obernsees-1. (z1), Werra Formation; (z2), Staßfurt Formation; (z3), Leine Formation; Sw-Sk, Shallow-marine – Sabkha settings. Detailed legend lithology and sedimentary structures on Figs 5 to 7.

of the changes in fluvial style is not possible due to insufficient data availability. Braided fluvial beds form the Lower–Middle Buntsandstein of Obernsees-1 following on the late Zechstein meandering fluvial units. The onset of braided depositional settings is marked by the gradual decrease and disappearance of floodplain and reworked overbank elements, and by a coarsening-upward and thinning-upward tendency of the fluvial beds. The first occurrence of braided deposits is instead slightly above the PTB in Lindau-1, marked by an abrupt facies change from dominantly sabkha elements and erosional contact. Both Lower Buntsandstein sequences define a gradual upward increase of braided fluvial gravel bars over sandy bedforms and occasional mass flow interbeds upsection, reflecting base-level fall. The overall coarsening-upward tendency and the dominance of cross-bedding over 'flashy' plane-lamination indicate higher, rather continuous sediment/water discharge, identifying a more perennial fluvial regime. Upward the increase of sand-dominated depositional elements, the disappearance of gravel-bars coupled with a higher frequency of floodplain beds and the development of obvious fining-upward patterns, mark the establishment of higher-sinuosity stream conditions. This change in fluvial style is transitional and reflects a lowering in stream gradient, flow velocities and higher availability of abundant suspension load. The fluvial turnover is considered to start above the coarsest braided gravel bed and occurs diachronous between the two wells (Figs 8 and 9). Thus, meandering fluvial deposits form the Middle–Upper Buntsandstein (*Detfurth – Röt 3 Formation)* of Obernsees-1, whereas increased river sinuosity is recorded from the Lower–Middle Buntsandstein transition (uppermost *Bernburg – Volpriehausen Formation*) in Lindau-1. Fluvio-aeolian deposits complete the Upper Buntsandstein sequence recorded in Obernsees-1 (Fig. 9), although thin aeolian beds occur sporadically embedded in the underlying floodplain rich fluvial sequence.

SANDSTONE PETROGRAPHIC COMPOSITION

Ninety-nine thin sections were counted to understand the variability of the compositional assemblages across the Rotliegend–Buntsandstein interval. The results of the petrographic point-count are reported in percentage as a function of the total amount of framework components (Table 3) in Obernsees-1 (OS) and Lindau-1 (LN) and indicated as subscript to the well abbreviations (for example, OS_{xx}; LN_{xx}). The detailed results of the point-count analysis are included as supplementary material (Table S1).

Upper Rotliegend

Upper Rotliegend samples consist of moderately to poorly sorted medium-sized (roS) to coarse-grained (roF) sandstones, with angular to very angular grains. Quartz is the main constituent occurring as monocrystalline (OS_{15}; LN_{31}), subordinate polycrystalline (OS_9; LN_1) and in phaneritic grains (OS_{36}; LN_{41}) (Figs 10A, 11A and 11C). Feldspars form between 10% and 20% of the framework in both wells and display moderate kaolinite and sericite alteration (Fig. 10A and 10B). K-feldspars are particularly abundant in Obernsees-1 (P/F $OS_{0.25}$; $LN_{0.46}$) (Folk, 1974) (Fig. 12). Phaneritic grains form most of the framework and consist of gneissic (Rm) and subordinate granitoid fragments (Rg) (Figs 10E and 11D) (OS-$Rm_{60}Rg_8Lm_{32}$; LN-$Rm_{93}Rg_4Lm_3$). The Rg/Rg + Rm ratio increases upsection from 0.03 to 0.09 in the Upper Rotliegend (roS) of Lindau-1, whereas the Rg content is higher in the Upper Rotliegend of Obernsees-1 (Rg/Rg + Rm $OS_{0.10–0.17}$; $LN_{0.01–0.17}$) (Fig. 12). Obernsees-1 displays high contents of metapelitic (Lmp1-2) and metafelsic (Lmf1-2) fragments (29%), decreasing upward to 10% (Figs 10C, 11D and 12), whereas Lindau-1 displays occasional metafelsic (Lmf1-2) and schist (Lmf3-4) fragments (Fig. 10D). Sandstone rock fragments (Rs) (Fig. 10G) form about 6% of the framework composition in Obernsees-1, whereas sedimentary lithics (Ls) rarely occur in both wells (OS_1; $LN_{<1}$). Rare palaeo-volcanic microlithic grains occur in Obernsees-1. Micas, mud clasts and dense minerals occur in low concentrations.

Zechstein

Zechstein samples are moderately sorted, fine to medium sandstones. Quartz varieties include monocrystalline (OS_{42}; LN_{34}), polycrystalline (OS_{11}; LN_6) and phaneritic grains (OS_{13}; LN_{27}). K-feldspars (OS_{23}; LN_{23}) and plagioclases (OS_8; LN_8) often exhibit kaolinite and sericite alteration. Gneiss fragments dominate the phaneritic association (OS-$Rm_{80}Rg_{19}Lm_1$; LN-$Rm_{94}Rg_4Lm_2$)

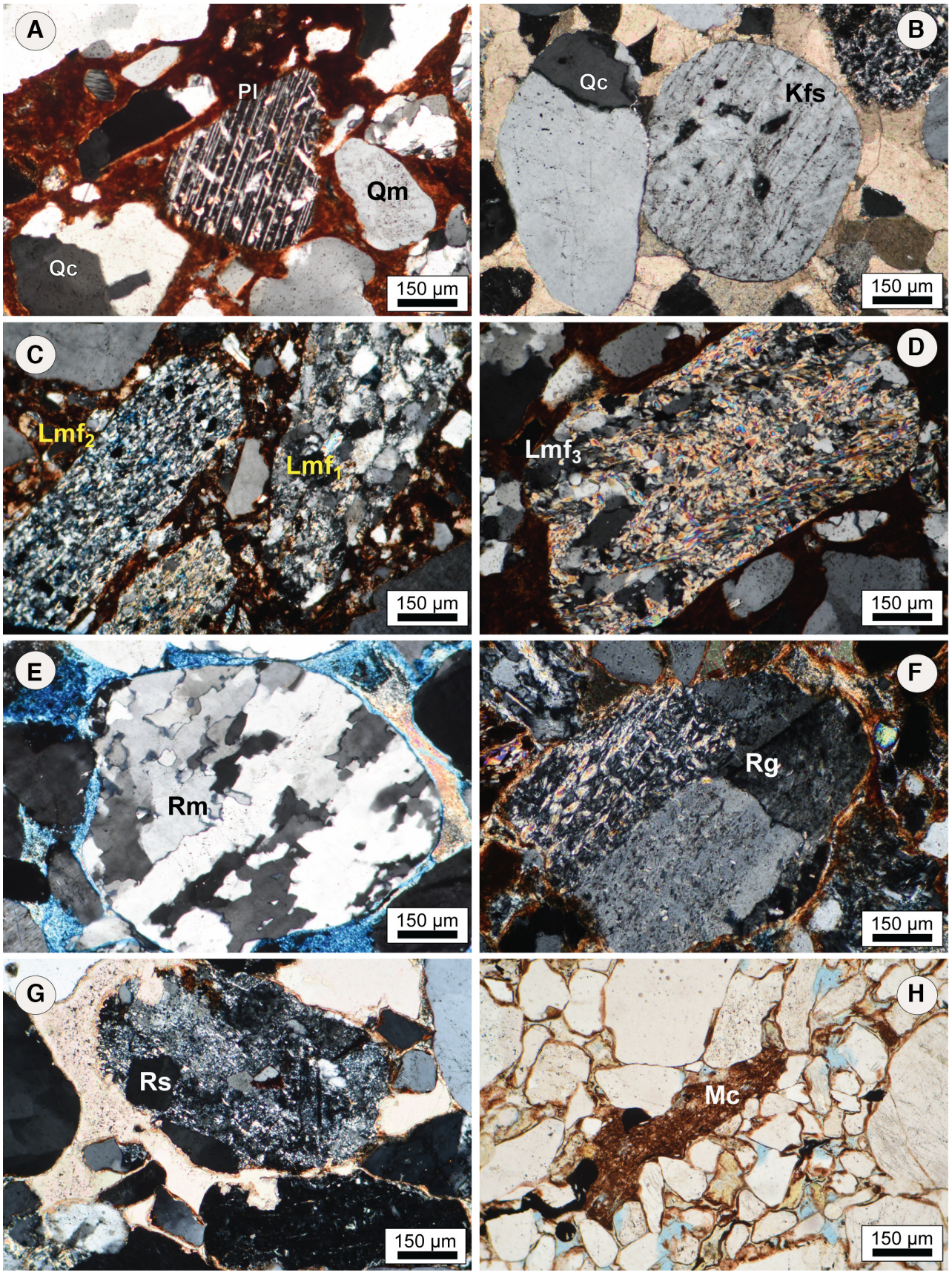

Fig. 10. Monomineralic grains and rock fragments. (A) Monocrystalline quartz (Qm), composite quartz >63 μm (Qc) and sericite alteration product on a polysynthetic-twinned plagioclase (Pl). (B) K-feldspar (Kfs) showing partial dissolution along the cleavage and associated Qc. (C) Low grade metafelsic lithic fragments (Garzanti & Vezzoli, 2003). Notice the increase of mica orientation associated with grain-size reduction from Lmf1 to Lmf2. (D) Schist rock fragment (Lmf3). (E) Gneissic and quartz dominated metamorphic rock fragment (Rm). (F) Feldspar-rich plutonic rock fragment (Rg). (G) Sandstone rock fragment (Rs). (H) Deformed mud-clast (Mc) squeezed between quartz grains.

(Fig. 11D), whereas the Rg content varies significantly across the Zechstein (Rg/Rg+Rm $OS_{0·08–0.41}$; $LN_{0.01–0.19}$) (Fig. 12). Metasedimentary lithics (Lmf1-2 and Lmp2), schist (Lmf3-4) and siltstones occur subordinately (<1%). Micas form about 1% of the framework component in both wells. Rs, mud clasts and dense minerals are accessory phases.

Lower Buntsandstein

Textural maturity varies from poorly-sorted to moderately-sorted, sub-rounded, fine to very coarse sandstones. Quartz occurs as monocrystalline (OS_{31}; LN_{27}), polycrystalline grains (OS_{14}; LN_3) and within phaneritic fragments (OS_{22}; LN_{37}). K-feldspar (OS_{23}; LN_{22}) and plagioclase (OS_7; LN_8) often display sericite and kaolinite alteration. Plagioclase content increases upward in Lindau-1 and becomes particularly abundant in specific stratigraphic levels of Obernsees-1 (P/F $OS_{0.09–0.43}$; $LN_{0.11–0.53}$) (Fig. 12). Rm grains dominate the phaneritic group in both wells (OS-$Rm_{76}Rg_{24}Lm_0$; LN-$Rm_{96}Rg_4Lm_0$), whereas the abundance of Rg (Fig. 10F) varies significantly in Obernsees-1 (Rg/Rg + Rm $OS_{0.07–0.47}$; $LN_{0–0.06}$) (Figs 11D and 12). Rs fragments occur rarely in Obernsees-1, while Ls and Lm form <1% in both wells. Deformed mud clasts acting as pseudo-matrix (OS_1; $LN_{<1}$) (Fig. 10H) and micas (OS_1; LN_1) are accessory. Dense minerals are rare.

Middle Buntsandstein

Sandstones are poorly to moderately sorted with sub-rounded grains, and an upward grain-size decrease from coarse to fine sand. Quartz occurs as monomineralic (OS_{35}; LN_{31}), polycrystalline grains (OS_{12}; LN_1) and within rock fragments (OS_{16}; LN_{32}) (Fig. 11A). K-feldspar (OS_{26}; LN_{23}) displays both partial diagenetic dissolution and kaolinite replacement. Plagioclase content varies between 2% and 12% in Obernsees-1 and forms about 11% of the framework in Lindau-1. Gneissic fragments dominate the phaneritic fraction in Lindau-1 (OS-$Rm_{75}Rg_{24}Lm_1$; LN-$Rm_{97}Rg_3Lm_0$) (Fig. 11D), whereas the relative abundance of granitoid and Rm varies significantly in Obernsees-1 (Rg/Rg + Rm $OS_{0.09–0.68}$; $LN_{0.02–0.03}$) (Fig. 12). Sandstone, siltstone and metafelsic fragments (Lmf1-3) only rarely occur in Obernsees-1 (<1%). Accessory components are micas, which locally reach up to 29% of the framework in Obernsees-1, and rare mud clasts and dense minerals (<1%).

Upper Buntsandstein

Samples from the lower part of the section are moderately sorted, medium to fine-grained sandstones, whereas those from the upper portion are well-sorted, medium to coarse sandstones. Roundness increases upward from sub-rounded to well-rounded. Quartz occurs as monomineralic (46%), polycrystalline grains (15%) and within phaneritic fragments (12%). Feldspars occur as both K-feldspar (19%), often showing kaolinite replacement, and plagioclase (7%), the latter with increasing abundance upsection (P/$F_{0.04–0.45}$) (Figs 10B and 12). Plagioclases do not exhibit particular alteration features. Gneissic fragments dominate the phaneritic association (Rg/Rg + Rm 0.11–0.43) (Fig. 12). Granitoids and metafelsic grains (Lmf2) are subordinate to rare ($Rm_{72}Rg_{28}Lm_0$) (Fig. 11D). Rs, mica and dense minerals are accessory (<1%).

DISCUSSION

Provenance changes across the Permian–Triassic boundary

Sandstones from both wells display a dominantly feldspatho–quartzose composition, except for the Upper Rotliegend of Obernsees-1, which is litho–feldspatho–quartzose/litho-quartzose (Fig. 11A). Accordingly, compositions reflect a predominantly transitional continental geodynamic

Table 3. Key petrographic parameters. Detailed point-count results in the supplementary material.

	Framework components (%)									
	Obernsees-1					Lindau-1				
	UR	Z	LB	MB	UB	UR(S)	UR(F)	Z	LB	MB
N°	*3*	*10*	*8*	*22*	*7*	*12*	*10*	*11*	*14*	*2*
Q	60	67	67	63	73	73	73	67	68	64
KF	16	23	23	26	19	13	13	23	22	23
P	4	8	7	5	7	11	11	8	8	11
M	1	1	1	4	1	2	2	1	1	2
Lm	18	<1	<1	<1	<1	1	2	<1	<1	0
Lv	<1	<1	0	0	0	0	0	0	0	0
Ls	1	<1	<1	<1	0	<1	<1	<1	<1	<1
Rc	0	0	0	0	0	0	0	0	<1	0
Mc	<1	<1	1	1	0	<1	<1	<1	<1	0
Pmtx	0	0	0	1	0	<1	<1	<1	<1	0
D	0	<1	<1	<1	<1	<1	0	<1	<1	0
Tot	100	100	100	100	100	100	100	100	100	100
Rm	31	14	21	16	10	50	48	31	45	37
Rg	4	2	7	5	4	2	2	1	2	1
Rv	0	0	0	0	0	<1	<1	0	0	0
Rs	6	<1	<1	<1	<1	0	0	0	0	0
aKF	3	3	3	6	3	2	1	2	2	2
aP	2	3	3	2	1	3	4	3	2	1
Qm	15	42	31	35	46	31	31	34	27	31
Qp	9	11	14	12	15	2	<1	6	3	1
Q-RF	26	13	22	16	12	40	42	27	37	32
Lmp^1	1	0	0	0	0	<1	<1	0	0	0
Lmp^2	0	0	<1	0	0	0	0	0	0	0
Lmp^3	0	0	0	0	0	<1	0	0	0	0
Lmp^4	0	0	0	0	0	0	<1	0	<1	0
Lmf^1	9	<1	<1	<1	0	1	<1	0	0	0
Lmf^2	8	<1	<1	<1	<1	<1	1	<1	0	0
Lmf^3	<1	<1	0	<1	0	<1	<1	<1	0	0
Lmf^4	0	0	0	0	0	0	<1	<1	0	0
MI	336	491	491	586	499	485	487	492	498	500
Rg/(Rm+Rg)	0.12	0.19	0.24	0.25	0.28	0.04	0.04	0.04	0.04	0.03
P/F	0.25	0.25	0.23	0.17	0.30	0.46	0.46	0.26	0.26	0.31
Ternary diagrams (%)										
QFL										
Q	60	68	68	67	74	74	74	68	69	65
F	21	32	31	33	26	24	24	31	31	35
L	19	0	1	0	0	2	2	1	0	0
QFRf										
Q	24	55	46	49	61	33	31	41	31	32
F	15	28	24	29	25	13	17	26	22	29
Rf	61	17	30	22	14	54	52	33	47	39
RmRgLm										
Rm	60	80	76	75	72	93	93	94	96	97
Rg	8	19	24	24	28	4	4	4	4	3
Lm	32	1	0	1	0	3	3	2	0	0

UR, Upper Rotliegend (S, roS; F, roF); Z, Zechstein; B, Buntsandstein (LB, Lower; MB, Middle; UB, Upper); N°, number of samples per unit; Q, total quartz; KF, total K-feldspar; P, total plagioclase; M, total mica; L, lithics (Lm, metamorphic; Lv, volcanic; Ls, sedimentary); Rc, extrabasinal carbonate; Mc, Mud clast; Pmtx, pseudomatrix; D, dense minerals; R, rock fragments (Rm, metamorphic; Rg, granitoids; Rv, volcanic; Rs, sedimentary); aK, altered K-feldspar; aP, altered plagioclase; Qm, monomineralic quartz; Qp, polycrystalline quartz; Q-RF, quartz in rock fragments; Lmp, metapelitic lithic (1–4 metamorphic rank); Lmf, metapsammite/metafelsite lithic (1–4 metamorphic rank); MI, metamorphic index (Garzanti & Vezzoli, 2003); Rg/(Rm+Rg), granitoids on gneisses ratio; P/F, plagioclase on total feldspar ratio (Folk, 1974); F, total feldspar; RF, phaneritic fragments.

setting (Dickinson, 1985) (Fig. 11B), whereas the abundance of metasedimentary lithics in the Rotliegend of Obernsees-1 points to a recycled orogen setting. Figure 11C illustrates the relationship between depositional settings and sandstone composition. Sandstones of the Rotliegend alluvial fans classify as feldspathic–litharenites and evolve to lithic-arkoses of the coastal meandering fluvial Zechstein deposits. A similar trend occurs in the Lower to Upper Buntsandstein sandstones following the evolution from coarse fluvial to aeolian systems. Therefore, compositional variations record changes in the depositional settings and are grain-size dependent. The downstream grain-size reduction determines Rf-rich coarse-grained proximal facies passing to monomineralic mineralogical assemblages dominating more distal settings. Upper Rotliegend sediments of Obernsees-1 display the highest content of low-grade metasediments (18%), which gradually decrease and finally disappear in the Zechstein (Fig. 12). The Upper Rotliegend metamorphic index (MI 277−395) (Fig. 11E) indicates erosion of mixed low-grade and high-grade metamorphic rocks (Garzanti & Vezzoli, 2003; Caracciolo *et al.*, 2015). Ediacaran low-grade metasedimentary rocks belong to the Saxo–Thuringian basement underlying the sedimentary succession of Obernsees-1 (Wall *et al.*, 2019). The upward increase of the MI (441–500) (Fig. 11E) supports both: (i) the unroofing of the Ediacaran metasediments and subsequent increasing exposure of gneissic lithologies; and/or (ii) drainage adjustments in response to fault activity. Low-grade metasediments rarely occur in Lindau-1. The MI constantly exceeds 441, indicating provenance from high-grade metamorphic terrains of the Bohemian Massif (BM). Nevertheless, low-grade metasediments are found in low concentrations at the roS–roF transition (Fig. 12), likely reflecting a regional tectonic event that created subsidence and accommodation space in the south-east *Kraichgau* area and drainage modifications in the *Naab* Basin. Such Permian synsedimentary tectonism is extensively discussed in the literature and linked to the establishment of a transtensional regime along the WBZ (Mattern *et al.*, 1995b; Peterek *et al.*, 1997; Schröder *et al.*, 1997; Siebel *et al.*, 2010). The succession of Obernsees-1 is richer in Rg fragments across the Zechstein–Buntsandstein boundary and in the Middle Buntsandstein. Higher granitic clast abundance corresponds to higher plagioclase contents, hence reflecting inputs from plagioclase-rich granitic sources (Fig. 12). The same features are visible in Lindau-1, although the lower Rg abundances there indicate less influence from granitic sources. We interpret the occurrence of granitic input at different stratigraphic levels to reflect local tectonic perturbations and consequent increase of sediment supply from unroofed Hercynian plutons. Zircon fission-tracks (Hejl *et al.*, 1997) and the occurrence of hydrothermal mineralization along WBZ (Mattern, 1995a; Peterek *et al.*, 1997; Siebel *et al.*, 2010) support the Early Triassic synsedimentary tectonism and unroofing of the western BM.

Drainage evolution and implications for the tectonic and climate reconstruction

The integration of sedimentological and compositional data sheds light on the processes controlling the regional sedimentary evolution across the PTB. In the following section, the forcing controls are discussed, comparing the environmental changes between the two wells for each lithostratigraphic interval (Fig. 4).

Based on the distribution of breccia deposits, Helmkampf (2006) assumed that the sediments of Lindau-1 and Obernsees-1 belong to the same depocentre from the uppermost Rotliegend onward. The data provided herein point to two distinct drainages and contrasting evolutions. The Rotliegend of Obernsees-1 represents the proximal–medial portions of mass flow-dominated alluvial fan systems (*sensu* Blair & McPherson, 1994), which form on steep topography (1.5° to 25°) with axial radial fan lengths <15 km (Stanistreet & McCarthy, 1993) (Fig. 13). No information is available on the lateral extent of the Obernsees-1 fan. Nevertheless, the compositional assemblage resulting from the erosion of the basement underneath the Upper Rotliegend beds indicates proximity to the source, therefore supporting the environmental interpretation. Fluvial fan systems are instead traditionally associated with more gentle topographic gradients and lengths up to several tens of kilometres (Moscariello, 2018). Accordingly, the presence of braided fluvial fans in Lindau-1 may reflect a more distant source located in the high-grade metamorphic units of the Saxo–Thuringian terrain. A dominantly transtensional tectonic regime established during the Rotliegend deposition along the Western Border fault Zone (WBZ) (Mattern, 1995a,b; Peterek *et al.*, 1997; Schröder *et al.*, 1997). Accordingly, synsedimentary tectonic perturbations led to the exhumation and following denudation of the basement bodies feeding the drainages in the *Naab* Basin and ultimately

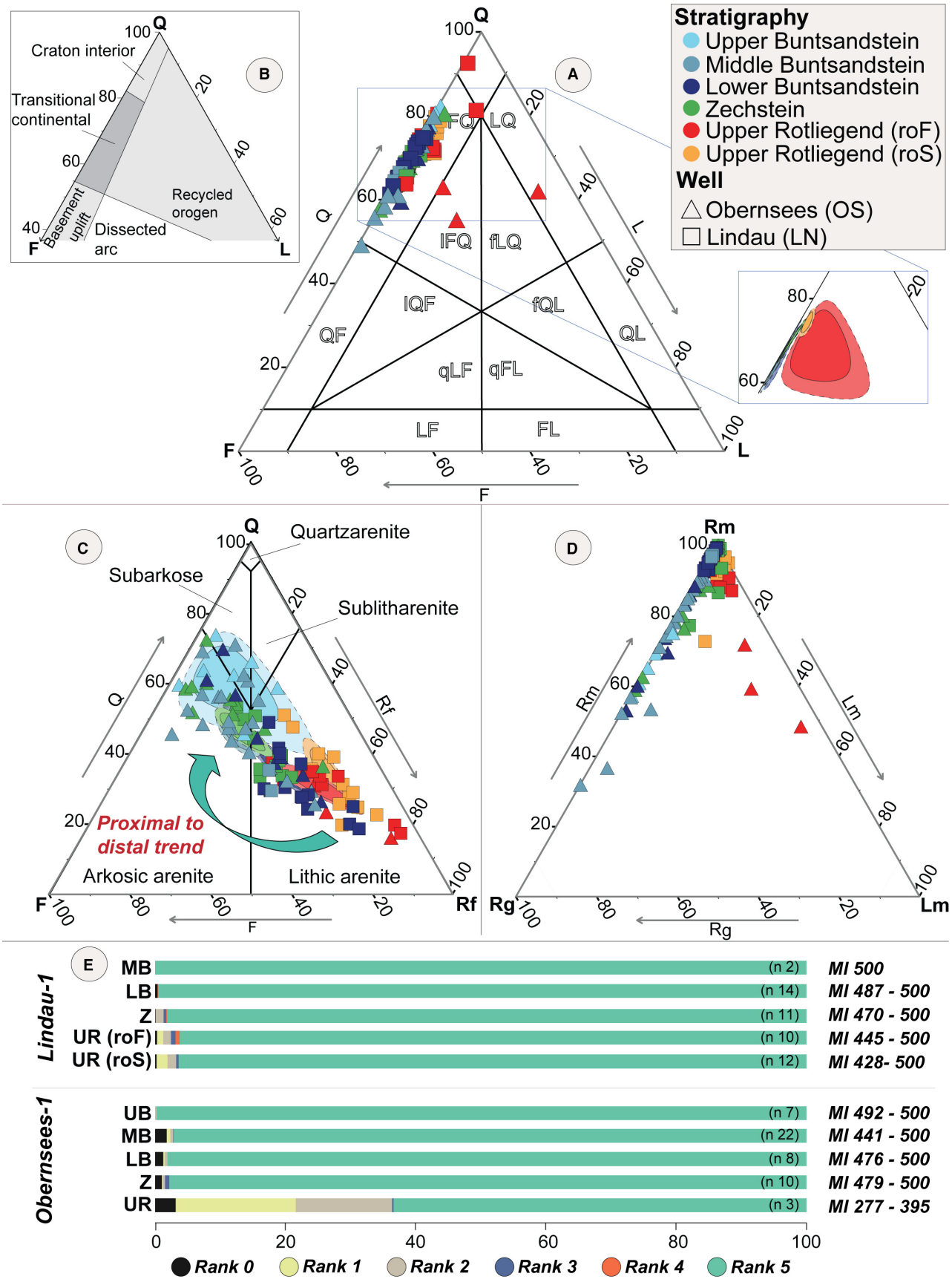

Fig. 11. Ternary diagrams for the 99 selected samples (50 Obernsees-1, 49 Lindau-1). Compositions listed in Table 3. (A) QFL plot = Quartz, Feldspar, Lithic fragments (Garzanti, 2018). Confidence regions illustrated to the right (99% – dashed outline; 95% – straight outline). (B) Tectonic discrimination diagram (Dickinson, 1985). (C) QFRf plot = Quartz, Feldspar, Rock Fragments (Pettijohn *et al.*, 1987; Caracciolo *et al.*, 2014). Confidence regions in the background. (D) RmRgLm plot = high-grade metamorphic rock fragments, granitoid fragments, low-grade metamorphic grains. (E) Metamorphic indexes (MI) (Garzanti & Vezzoli, 2003) by units. UR, Upper Rotliegend; Z, Zechstein; B, Buntsandstein (LB, Lower; MB, Middle; UB, Upper). Metamorphic ranks = 0 (no metamorphism), 1 (very low grade), 2 (low grade), 3 (medium grade), 4 (high-grade), 5 (very high grade); n, number of samples for unit.

resulting in the braided fluvial fan progradation recorded in Lindau-1. In the same way, local tectonism favoured the increase of sediment supply, unroofing of Ediacaran metasediments and further creation of accommodation space in the Obernsees-1 drainage (Fig. 13). Furthermore, the fluvial fan–sabkha interactions in the Rotliegend of Lindau-1 (Fig. 8) support tectonic fluctuations with quiescent phases triggering the retrogradation of the coastal system.

Cycles attributed to base-level rise at the Rotliegend–Zechstein transition of both wells (Fig. 12) result from increasing sediment storage capacities during repetitive transgressions of the Zechstein sea (Schuh, 1985; Paul, 2006). The fan-delta to shallow-marine sequence of Obernsees-1 is temporarily interrupted by the restoration of continental sandflat environments (Fig. 9), likely reflecting higher frequency sea-level oscillations (Schuh, 1985). Upsection, Obernsees-1 exhibits a clear regressive tendency and a shift to fluvially controlled deposition mirroring the trends identified in other portions of the Central European Basin System (CEBS) (Aigner & Bachmann, 1992; Aigner *et al.*, 1999; Bachmann *et al.*, 2008). The establishment of meandering wet plains in the marginal, more terrestrial environments surrounding the Zechstein sea is attributed to increased humid conditions and precipitation, triggered by the enhanced evaporation of the large epicontinental sea (Roscher & Schneider, 2006; Summerhayes, 2015). The regressive tendency is less obvious across the Zechstein of Lindau-1, where the Buntsandstein braided sequence erosionally overlays the Zechstein coastal deposits. A stratigraphic unconformity marking the Permian–Triassic in the *Naab* area is speculated in Peterek *et al.* (1997), who indicate pronounced uplift events of the western BM induced by the stress reversal of the *Franconian Line* and *Pfahl Fault*. Accordingly, the abrupt facies change at the PTB of Lindau-1 may result from this tectonic phase. However, Buntsandstein fluvial conglomerates and sandstones unconformably overlie the uppermost Zechstein deposits in several other marginal areas of the CEBS, pointing to a more regional rather than local event (Bourquin *et al.*, 2007; Stollhofen *et al.*, 2008). Our data suggest the existence of distinct depositional conditions during the Zechstein between the two wells. Lindau-1 deposition occurred in a more marginal area dominated by coastal facies aggradation, although the unconformable facies change at the PTB questions the vertical continuity of the sequence. Conversely, the Zechstein evolution of Obernsees-1 appears continuous and more influenced by the base-level and climate variations as documented in the rest of the CEBS (Fig. 13).

The Lower Buntsandstein sequences of both wells record the onset of coarse-grained braided systems followed by a fluvial style turnover and enhanced river sinuosity throughout the Middle–Upper Buntsandstein (Fig. 12). This evolution differs from the trends described in central portions of the CEBS, where lacustrine beds are gradually replaced by prograding aeolian and fluvial belts, resulting in an overall regressive pattern (Paul, 1982; Bachmann *et al.*, 2009). Many authors attributed the sedimentary evolution in the distal CEBS to reflect base-level fluctuations of the large endorheic lake occupying the basin centre (Geluk & Röhling, 1997; Palermo *et al.*, 2008; Voigt *et al.*, 2011). However, the proximal position of the successions in the east Franconian Basin is more likely to reflect upstream controls on the sedimentation, either resulting from syndepositional tectonism or climate (Caracciolo, 2020). The differences in the compositional assemblages and sedimentary evolutions between the two wells (Fig. 12) indicate the persistence of two distinct drainages during the Buntsandstein. The more frequent arrival of granitic components in Obernsees-1 coeval with influxes of coarse-grained detritus and onset of fluvial deposition supports the role of tectonism, pointing to the local exhumation and erosion of plutonic bodies. A phase of active Early Triassic tectonism in south-east

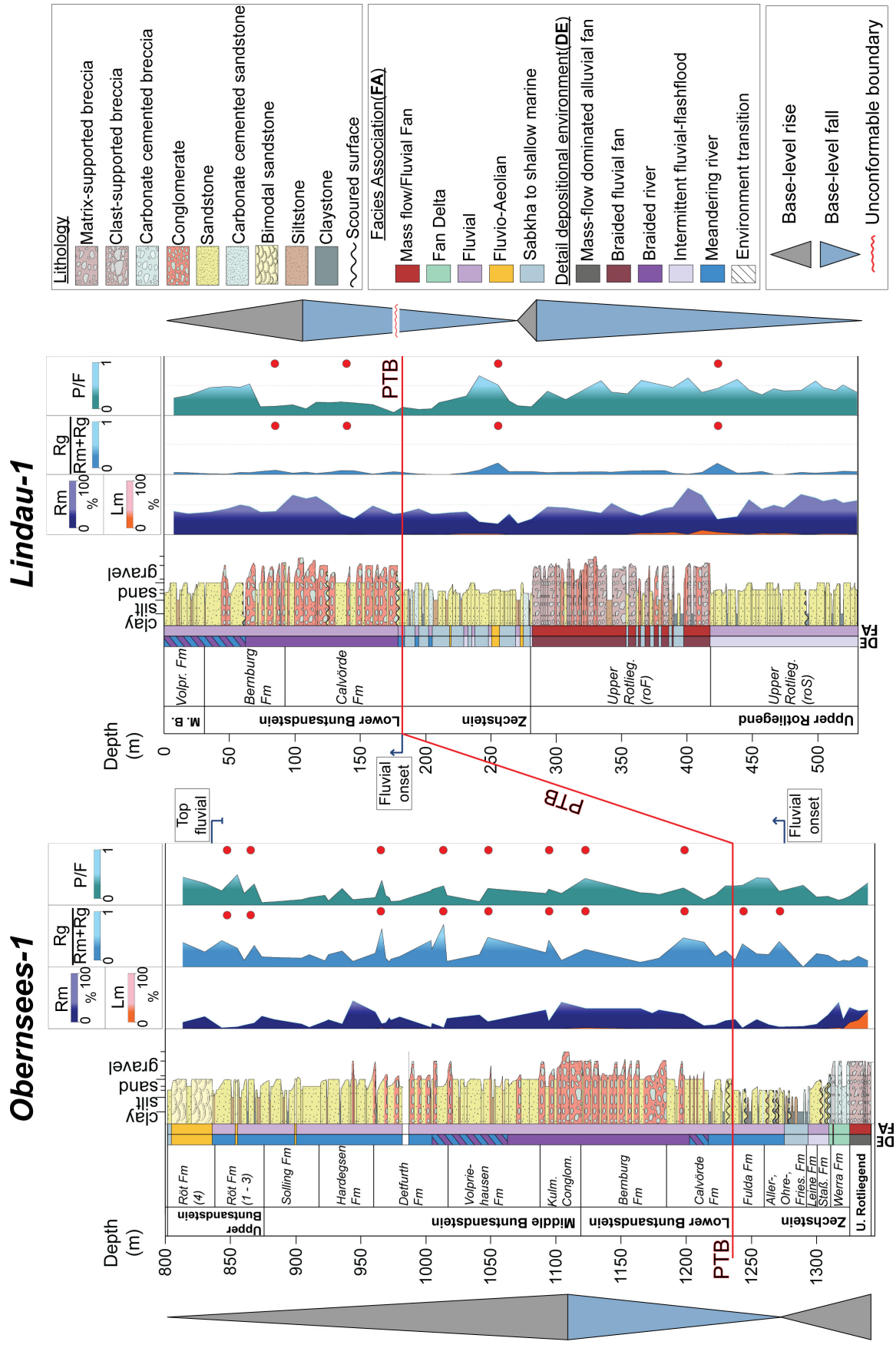
Lithology
Matrix-supported breccia
Clast-supported breccia
Carbonate cemented breccia
Conglomerate
Sandstone
Carbonate cemented sandstone
Bimodal sandstone
Siltstone
Claystone
Scoured surface
Facies Association(FA)
Mass flow/Fluvial Fan
Fan Delta
Fluvial
Fluvio-Aeolian
Sabkha to shallow marine
Detail depositional environment(DE)
Mass-flow dominated alluvial fan
Braided fluvial fan
Braided river
Intermittent fluvial-flashflood
Meandering river
Environment transition
Base-level rise
Base-level fall
Unconformable boundary
Lindau-1
Obernsees-1
Depth (m)
clay
silt
sand
gravel
Rm
Lm
Rg
Rm+Rg
P/F
PTB
Fluvial onset
Top fluvial
M. B.
Lower Buntsandstein
Zechstein
Upper Rotliegend
U. Rotliegend
Middle Buntsandstein
Upper Buntsandstein
Volpr. Fm
Bernburg Fm
Calvörde Fm
Upper Rotlieg. (roF)
Upper Rotlieg. (roS)
Röt Fm (4)
Röt Fm (1 - 3)
Solling Fm
Hardegsen Fm
Detfurth Fm
Volpriehausen Fm
Kulm. Conglom.
Fulda Fm
Aller-, Ohre-, Fries. Fm
Leine Fm
Stass. Fm
Werra Fm
DE
FA

Fig. 12. Sedimentological logs of Obernsees-1 and Lindau-1 and petrographic indexes of provenances: Rm, high-grade metamorphic rock fragments; Lm, low-grade metamorphic grains; Rg, granitoid fragments; P, plagioclase; F, total feldspars. The logs are compared according to the lithostratigraphic frameworks (Fig. 4). Environmental and grain-size tendencies are discussed in the text and defined according to the lithostratigraphic schemes. Notice the diachronous change in fluvial style at the Lower–Middle Buntsandstein transition in Obernsees-1 and during the Lower Buntsandstein in Lindau-1. Red dots indicate levels with high abundance in Rg and P.

Germany is associated with the reactivation of several north-west/south-east striking faults of the WBZ (Klare *et al.*, 1995; Mattern, 1995a; Peterek *et al.*, 1997; Schröder *et al.*, 1997; Siebel *et al.*, 2010). Whether the regime was compressional or extensional is still a matter of debate and cannot be inferred from our investigation. Nevertheless, the low granitic contribution in Lindau-1 and the diachronous fluvial evolution point to a non-contemporaneous reactivation of different Variscan faults regulating the sedimentation in the regions sampled by the two wells. Hence, the sedimentary patterns described for the Buntsandstein of the Franconian Basin may reflect phases of synsedimentary fault activity affecting sediment supply.

If the compositional signatures support the role of tectonics from one side, on the other

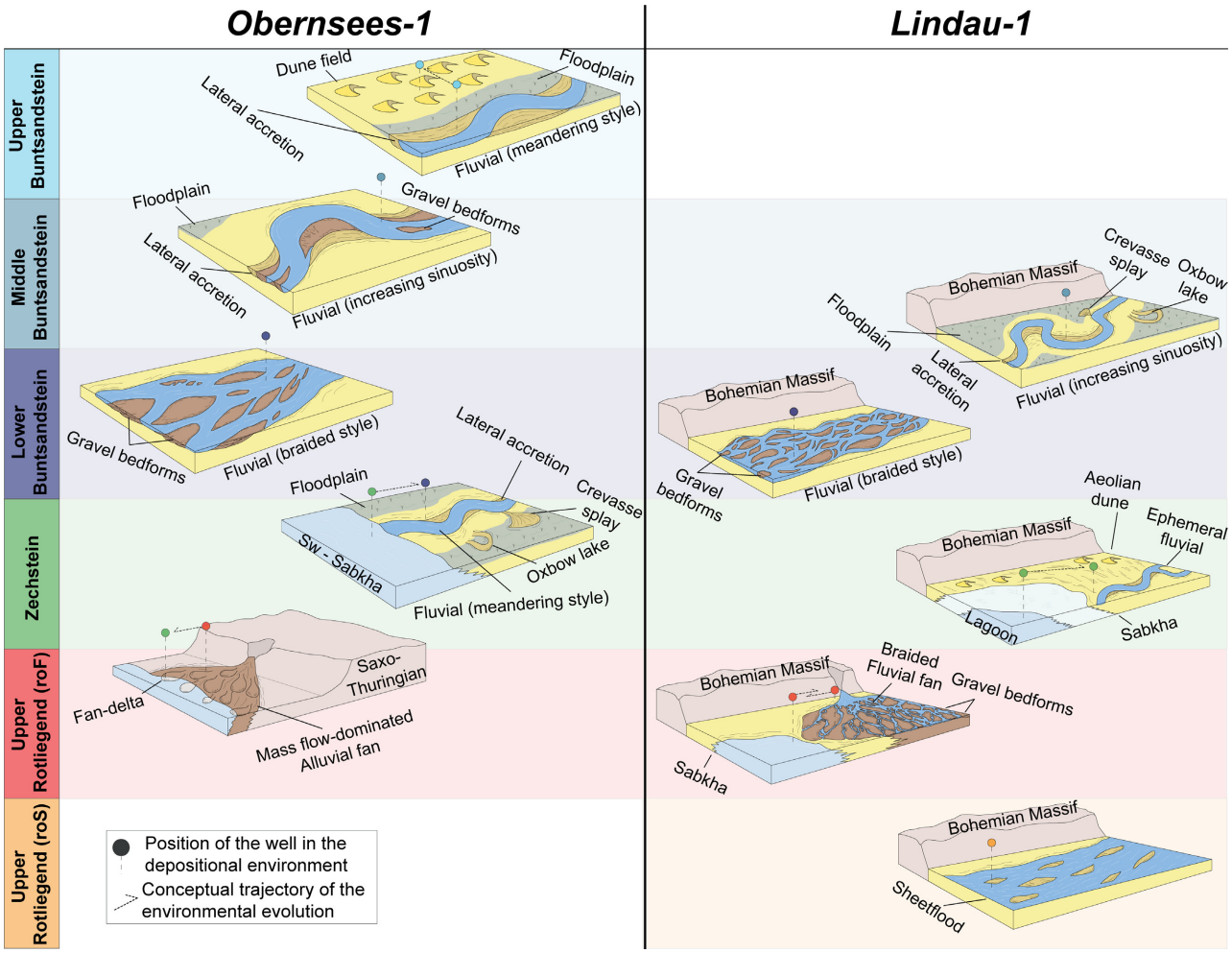

Fig. 13. Conceptual models showing the sedimentary evolution described for the wells Obernsees-1 and Lindau-1 across the Permian – Early Triassic interval. The successions are compared on the base of the lithostratigraphic frameworks.

side, Figure 12 illustrates that higher inputs from granitic sources occur across the entire Buntsandstein of Obernsees-1 regardless of the major changes in fluvial style. Therefore, active tectonism is not sufficient to solely explain the fluvial progradation documented at the PTB in both wells. The perennial nature of the Early Buntsandstein braided systems instead points to a climatic contribution on the Triassic evolution of the Franconian Basin. The transition from meandering/sabkha to gravel/sandy-dominated braided systems is well-known in several PTB sections worldwide (Zhu *et al.*, 2020, and references therein). Newell *et al.* (1999) and Ward *et al.* (2000) attributed the fluvial change to the riparian vegetation die-back event, resulting in riverbank instability and facilitated erosion. Increased aridity and mass wasting are identified as the main triggers on the fringing vegetation turnover (Benton & Newell, 2014). Besides, increased sediment fluxes at the PTB are speculated as result of enhanced chemical weathering triggered by higher temperature, increased rainfall acidity and mass wasting of soils and bedrocks (Algeo & Twitchett, 2010; Algeo *et al.*, 2011). Several studies suggest that the environmental evolution in the CEBS is somewhat controlled by climatic perturbations (Péron *et al.*, 2005; Roscher *et al.*, 2011). Based on the investigation of lacustrine deposits from central Germany, Hiete *et al.* (2006) and Käsbohrer & Kuss (2021) inferred temporary positive shifts in the water balance across the PTB, either resulting from increased precipitation/water inflow or reduced evaporation. The occurrence of braided rivers with highly variable discharge in the arid Early Triassic of the Paris Basin (France) and Holy-Cross Mountains (Poland) has been attributed to seasonal precipitation and increased water influxes from the nearby Hercynian reliefs (Bourquin *et al.*, 2009; Jewuła *et al.*, 2020a). Given the proximal position of Obernsees-1 and Lindau-1 to the catchment area (BM), uphill wetter conditions would support both the fluvial progradation across the PTB and the more perennial nature of drainages with a braided pattern. Parrish (1993) highlights that constant rainfall is not necessary to maintain a perennial fluvial regime as long as the total annual precipitation is high. Seasonal extreme precipitations related to monsoonal circulation have been modelled for the circum-Tethyan region during the Early Triassic (Kutzbach & Gallimore, 1989; Zwan & Spaak, 1992; Roscher *et al.*, 2011). The close position of the BM to the Neothethys may have favoured the entrapment of moisture, leading to wetter conditions on the uphill catchment area and resulting in higher sediment discharge to the Franconian Basin. A similar case is described for the Late Triassic Chinle Formation (Colorado), where perennial rivers flowing in an arid basin were fed by the wetter surrounding highlands exposed to seasonal monsoon circulations (Blakey & Gubitosa, 1984; Dubiel *et al.*, 1991).

CONCLUSIONS

The combination of sedimentological and petrographic data provides key indications to answer some of the most debated questions regarding the Permian–Triassic sedimentary evolution of the south-east margin of the Central European Basin System (CEBS).

- This study supports the existence of two distinct depositional systems during the Rotliegend–Buntsandstein interval, challenging previous models. Compositional data and metamorphic indices indicate the existence of at least two distinct detrital sources. Both sequences received a constant supply dominantly from metamorphic lithologies. High-grade and subordinate medium-grade metamorphic rocks characterize Lindau-1. Compositions in the Obernsees-1 core indicate a more variegated assemblage of basement lithologies and record the drainage evolution through time. During the Rotliegend, Obernsees-1 was sourced by mixed high-grade and low-grade metamorphic rocks. The latter signal disappears across the Zechstein and Buntsandstein interval, where several peaks of granitic clast occurrences reflect the increasing unroofing and erosion of Variscan granitoids. Such pulses are also documented in Lindau-1, however, with a considerably lower role. The catchment feeding Lindau-1 is most likely located in the Saxo–Thuringian terrain of the Bohemian Massif (BM), whereas the source area of Obernsees-1 is not yet constrained.
- Sedimentological and compositional evidence point to dominantly climatic and tectonic controls on the sedimentary evolution across the Permian–Triassic, with minor influence from base-level fluctuations. The reactivation of Variscan faults has a key role during the Rotliegend mass flow/fluvial fan phase, leading to exhumation and denudation of various basement bodies, in turn increasing the sediment flux to the basin. The

effects of the marine transgressions and base-level fluctuations are constrained in the Zechstein of Obernsees-1, whereas the less pronounced effects in Lindau-1 suggest a more isolated depositional area. The overall regressive phase documented by the onset of perennial braided rivers across the Permian–Triassic Boundary (PTB) is indicative of a general increase in water inflow to the basin associated with a seasonally wetter source area. Nevertheless, the different compositional signatures, diachronous sedimentary evolution and the unconformity marking the PTB in Lindau-1 support the major role of tectonism during the Buntsandstein, resulting from diverse and non-contemporaneously active faults.

ACKNOWLEDGEMENTS

The authors thank their collaborators at the Bayerisches Landesamt für Umwelt (LfU) at Hof for kindly providing the samples used in this study, and for supporting core logging and complementary sampling. The authors declare no conflict of interest. The authors are very grateful to Professor César Viseras and five anonymous reviewers for the critical constructive review and suggestions that helped to improve the final version of the manuscript. The authors also thank Conwy Valley Systems Limited for providing great support with the PETROG^{TM} software used for the collection of petrographic data.

DATA AVAILABILITY STATEMENT

The data that support the findings of this study are available within the article and its supplementary materials.

REFERENCES

Aigner, T. and **Bachmann, G.H.** (1992) Sequence-stratigraphic framework of the German Triassic. *Sed. Geol.*, **80**, 115–135.

Aigner, T., **Hornung, J.**, **Junghans, W.D.** and **Pöppelreiter, M.** (1999) Baselevel cycles in the Triassic of the South-German Basin: a short progress report. *Zbl. Geol. Paläontol.*, **7**, 537–544.

Aitchison, J. (1997) The one-hour course in compositional data analysis or compositional data analysis is simple. In: *Proceedings of IAMG'97: the third annual conference of the International Association for Mathematical Geology, International Center for Numerical Methods in Engineering (CIMNE)*, Barcelona, Spain, 3–35.

Algeo, T.J., **Chen, Z.Q.**, **Fraiser, M.L.** and **Twitchett, R.J.** (2011) Terrestrial–marine teleconnections in the collapse and rebuilding of Early Triassic marine ecosystems. *Palaeogeogr. Palaeoclimatol. Palaeoecol.*, **308**, 1–11.

Algeo, T.J. and **Twitchett, R.J.** (2010) Anomalous Early Triassic sediment fluxes due to elevated weathering rates and their biological consequences. *Geology*, **38**, 1023–1026.

Allen, J.P., **Fielding, C.R.**, **Rygel, M.C.** and **Gibling, M.R.** (2013) Deconvolving signals of tectonic and climatic controls from continental basins: an example from the Late Paleozoic Cumberland Basin, Atlantic Canada. *J. Sed. Res.*, **83**, 847–872.

Amiel, A.J. and **Friedman, G.M.** (1971) Continental sabkha in Arava Valley between Dead Sea and Red Sea: significance for origin of evaporites. *AAPG Bulletin*, **55**, 581–592.

Antrett, P. (2013) *Characterization of an Upper Permian Tight Gas Reservoir*. Springer, Berlin, 114 pp.

Augustsson, C., **Aehnelt, M.**, **Voigt, T.**, **Kunkel, C.**, **Meyer, M.** and **Schellhorn, F.** (2019) Quartz and zircon decoupling in sandstone: Petrography and quartz cathodoluminescence of the Early Triassic continental Buntsandstein Group in Germany. *Sedimentology*, **66**, 2874–2893.

Augustsson, C., **Voigt, T.**, **Bernhart, K.**, **Kreißler, M.**, **Gaupp, R.**, **Gärtner, A.**, **Hofmann, M.** and **Linnemann, U.** (2018) Zircon size-age sorting and source-area effect: The German Triassic Buntsandstein Group. *Sed. Geol.*, **375**, 218–231.

Bachmann, G.H., **Hauschke, N.** and **Kozur, H.W.** (2009) *6th International Field Workshop. Buntsandstein Cyclicity and Conchostracan Biostratigraphy of the Halle (Saale) Area, Central Germany*, September 12–13, 2009, 30 pp.

Bachmann, G.H., **Voigt, T.**, **Bayer, U.**, **von Eynatten, H.**, **Legler, B.** and **Littke, R.** (2008) Depositional history and sedimentary cycles in the Central European Basin System. In: *Dynamics of Complex Intracontinental Basins: The Example of the Central European Basin System* (Eds Littke, R., Bayer, U., Gajewski, D. and Nelskamp, S.), pp. 156–172. Springer, Berlin.

Bailey, E.H. and **Stevens, R.E.** (1960) Selective staining of K-feldspar and plagioclase on rock slabs and thin sections. *Am. Mineral.*, **45**, 1020–1025.

Benton, M.J. and **Newell, A.J.** (2014) Impacts of global warming on Permo-Triassic terrestrial ecosystems. *Gondwana Res.*, **25**, 1308–1337.

Bindig, M. and **Backhaus, E.** (1995) Rekonstruktion der Paläoenvironments aus den fluviatilen Sedimentkörpern der Röt-Sandsteinfazies (Oberer Buntsandstein) Südwestdeutschlands. *Geol. Jahr. Hessen*, **123**, 69–105.

Black, B.A., **Neely, R.R.**, **Lamarque, J.-F.**, **Elkins-Tanton, L.T.**, **Kiehl, J.T.**, **Shields, C.A.**, **Mills, M.J.** and **Bardeen, C.** (2018) Systemic swings in end-Permian climate from Siberian Traps carbon and sulfur outgassing. *Nat. Geosci.*, **11**, 949–954.

Blair, T.C. and **McPherson, J.G.** (1994) Alluvial fans and their natural distinction from rivers based on morphology, hydraulic processes, sedimentary processes, and facies assemblages. *J. Sed. Res.*, **64**, 450–489.

Blakey, R.C. and **Gubitosa, R.** (1984) Controls of sandstone body geometry and architecture in the Chinle Formation (Upper Triassic), Colorado Plateau. *Sed. Geol.*, **38**, 51–86.

Bourquin, S., **Bercovici, A.**, **López-Gómez, J.**, **Diez, J.B.**, **Broutin, J.**, **Ronchi, A.**, **Durand, M.**, **Arché, A.**, **Linol, B.** and **Amour, F.** (2011) The Permian-Triassic transition and the onset of Mesozoic sedimentation at the northwestern peri-Tethyan domain scale: Palaeogeographic maps and

geodynamic implications. *Palaeogeogr. Palaeoclimatol. Palaeoecol.*, **299**, 265–280.

Bourquin, S., **Durand, M.**, **Diez, J.B.**, **Broutin, J.** and **Fluteau, F.** (2007) The Permian-Triassic boundary and Early Triassic sedimentation in Western European basins: an overview. *J. Ib. Geol.*, **33**, 221–236.

Bourquin, S., **Guillocheau, F.** and **Péron, S.** (2009) Braided rivers within an arid alluvial plain (example from the Lower Triassic, western German Basin): recognition criteria and expression of stratigraphic cycles. *Sedimentology*, **56**, 2235–2264.

Bourquin, S., **Peron, S.** and **Durand, M.** (2006) Lower Triassic sequence stratigraphy of the western part of the Germanic Basin (west of Black Forest): Fluvial system evolution through time and space. *Sed. Geol.*, **186**, 187–211.

Bourquin, S., **Rigollet, C.** and **Bourges, P.** (1998) High-resolution sequence stratigraphy of an alluvial fan–fan delta environment: stratigraphic and geodynamic implications–An example from the Keuper Chaunoy Sandstones, Paris Basin. *Sed. Geol.*, **121**, 207–237.

Bowman, D. (2019) *Principles of Alluvial Fan Morphology*. Springer, Dordrecht, 164 pp.

Briere, P.R. (2000) Playa, playa lake, sabkha: Proposed definitions for old terms. *J. Arid Environ.*, **45**, 1–7.

Burgess, S.D., **Muirhead, J.D.** and **Bowring, S.A.** (2017) Initial pulse of Siberian Traps sills as the trigger of the end-Permian mass extinction. *Nat. Commun.*, **8**, 164.

Calvache, M.L., **Viseras, C.** and **Fernández, J.** (1997) Controls on fan development—evidence from fan morphometry and sedimentology; Sierra Nevada, SE Spain. *Geomorphology*, **21**, 69–84.

Cao, Y., **Song, H.**, **Algeo, T.J.**, **Chu, D.**, **Du, Y.**, **Tian, L.**, **Wang, Y.** and **Tong, J.** (2019) Intensified chemical weathering during the Permian-Triassic transition recorded in terrestrial and marine successions. *Palaeogeogr. Palaeoclimatol. Palaeoecol.*, **519**, 166–177.

Caracciolo, L. (2020) Sediment generation and sediment routing systems from a quantitative provenance analysis perspective: Review, application and future development. *Earth-Sci. Rev.*, **207**, 103226.

Caracciolo, L., **Arribas, J.**, **Ingersoll, R.V.** and **Critelli, S.** (2014) The diagenetic destruction of porosity in plutoniclastic petrofacies: the Miocene Diligencia and Eocene Maniobra formations, Orocopia Mountains, southern California, USA. *Geol. Soc. Spec. Publ.*, **386**, 49–62.

Caracciolo, L., **Critelli, S.**, **Cavazza, W.**, **Meinhold, G.**, **von Eynatten, H.** and **Manetti, P.** (2015) The Rhodope Zone as a primary sediment source of the southern Thrace basin (NE Greece and NW Turkey): evidence from detrital heavy minerals and implications for central-eastern Mediterranean palaeogeography. *Int. J. Earth. Sci.*, **104**, 815–832.

Charton, R., **Bertotti, G.**, **Duval Arnould, A.**, **Storms, J.E.A.** and **Redfern, J.** (2020) Low-temperature thermochronology as a control on vertical movements for semi-quantitative Source-to-Sink analysis: A case study for the Permian to Neogene of Morocco and surroundings. *Basin Res.*, **33**, 1337–1383.

Chayes, F. (1952) Notes on the staining of potash feldspar with sodium cobaltinitrite in thin section. *Mineral. Soc. Am.*, **37**, 337–340.

Chu, D., **Yu, J.**, **Tong, J.**, **Benton, M.J.**, **Song, H.**, **Huang, Y.**, **Song, T.** and **Tian, L.** (2016) Biostratigraphic correlation and mass extinction during the Permian-Triassic transition in terrestrial-marine siliciclastic settings of South China. *Glob. Planet. Change.*, **146**, 67–88.

Clemmensen, L.B. (1985) Desert sand plain and sabkha deposits from the Bunter Sandstone Formation (L. Triassic) at the northern margin of the German Basin. *Geol. Rundsch.*, **74**, 519–536.

Clemmensen, L.B. and **Abrahmsen, K.** (1983) Aeolian stratification and facies association in desert sediments, Arran basin (Permian), Scotland. *Sedimentology*, **30**, 311–339.

Dickinson, W.R. (1985) Interpreting provenance relations from detrital modes of sandstones. In: *Provenance of Arenites* (Ed. Zuffa, G.C.), pp. 333–362. D. Reidel Publishing Company, Dordrecht.

Dill, H.G. and **Klosa, D.** (2011) Heavy mineral-based provenance analysis of Mesozoic continental-marine sediments at the western edge of the Bohemian Massif, SE Germany: with special reference to Fe–Ti minerals and the crystal morphology of heavy minerals. *Int. J. Earth. Sci.*, **100**, 1497–1513.

Donselaar, M.E. and **Overeem, I.** (2008) Connectivity of fluvial point-bar deposits: An example from the Miocene Huesca fluvial fan, Ebro Basin, Spain. *AAPG Bulletin*, **92**, 1109–1129.

Dubiel, R.F., **Parrish, J.T.**, **Parrish, J.M.** and **Good, S.C.** (1991) The Pangaean megamonsoon: evidence from the Upper Triassic Chinle Formation, Colorado Plateau. *Palaios*, **6**(4), 347–370.

Emmert, U., **Gudden, H.**, **Haunschild, H.**, **Meyer, R.K.**, **Schmid, H.**, **Schuh, H.**, **Stettner, G.** and **Risch, H.** (1985) Bohrgut-Beschreibung der Forschungsbohrung Obernsees. *Geol. Bavar.*, **88**, 23–47.

Erwin, D.H. (1994) The Permo-Triassic extinction. *Nature*, **367**, 231–236.

Eugster, H.P. (1980) Geochemistry of evaporitic lacustrine deposits. *Ann. Rev. Earth Planet. Sci.*, **8**, 35–63.

Fernández, J., **Bluck, B.J.** and **Viseras, C.** (1993) The effects of fluctuating base level on the structure of alluvial fan and associated fan delta deposits: an example from the Tertiary of the Betic Cordillera, Spain. *Sedimentology*, **40**, 879–893.

Folk, R.L. (1974) *Petrology of Sedimentary Rocks*. Hemphill Publishing Company, Austin, 184 pp.

Fraser, G.S. and **Suttner, L.** (1986) *Alluvial Fans and Fan Deltas: A Guide To Exploration for Oil and Gas*. Prentice Hall, Boston, MA, 199 pp.

Freudenberger, W., **Friedlein, V.**, **Schulze, M.** and **Sprecht, S.** (2016) Kernbohrungen in der Trias Unterfrankens. *Geologica Bavarica*, **114**, 125 pp.

Freudenberger, W., **Geyer, G.** and **Schröder, B.** (2014) Der Buntsandstein im nördlichen Bayern (nordwestliches Franken, Bruchschollenland und Randfazies im Untergrund). In: *Deutsche Stratigraphische Kommission, Stratigraphie von Deutschland XI, Buntsandstein* (Eds Lepper, J. and Röhling, H.-G.), *Schriftenr. Dt. Ges. Geowiss.*, **69**, 547–582.

Freudenberger, W. and **Schwerd, K.** (1996) *Erläuterungen zur Geologischen Karte von Bayern 1. Geol. :500000*. Bayerisches Geologisches Landesamt, München, 329 pp.

Frostick, L.E. and **Reid, I.** (1977) The origin of horizontal laminae in ephemeral stream channel-fill. *Sedimentology*, **24**, 1–9.

Fryberger, S.G. and **Schenk, C.J.** (1988) Pin stripe lamination: a distinctive feature of modern and ancient eolian sediments. *Sed. Geol.*, **55**, 1–15.

Galloway, W.E. and **Hobday, D.K.** (2012) *Terrigenous Clastic Depositional Systems: Applications to Petroleum, Coal, and Uranium Exploration*. Springer Science & Business Media, New York, NY, 423 pp.

García-García, F., **Corbí, H.**, **Soria, J.M.** and **Viseras, C.** (2011) Architecture analysis of a river flood-dominated delta during an overall sea-level rise (early Pliocene, SE Spain). *Sed. Geol.*, **237**, 102–113.

Garzanti, E. (2018) Petrographic classification of sand and sandstone. *Earth-Sci. Rev.*, **192**, 545–563.

Garzanti, E. and **Vezzoli, G.** (2003) A Classification of metamorphic grains in sands based on their composition and grade. *J. Sed. Res.*, **73**, 830–837.

Gastaldo, R.A., **Neveling, J.**, **Clark, C.K.** and **Newbury, S.S.** (2009) The terrestrial Permian-Triassic boundary event bed is a nonevent. *Geology*, **37**, 199–202.

Geluk, M.C. (2005) *Stratigraphy and Tectonics of Permo-Triassic Basins in the Netherlands and Surrounding Areas*. PhD Dissertation. Utrecht University, Utrecht, 171 pp.

Geluk, M.C. and **Röhling, H.-G.** (1997) High-resolution sequence stratigraphy of the Lower Triassic 'Buntsandstein' in the Netherlands and northwestern Germany. *Neth. J. Geosci.*, **76**, 227–246.

Geluk, M.C. and **Röhling, H.-G.** (2016) A tectono-stratigraphic model for the depositional history and basin development of the Permian-Early Triassic at the southern margin of the Southern Permian Basin (The Netherlands and adjacent parts of Belgium and Germany). *Z. Dt. Ges. Geowiss.*, **167**, 149–166.

George, G.T. and **Berry, J.K.** (1993) A new lithostratigraphy and depositional model for the Upper Rotliegend of the UK Sector of the Southern North Sea. *Geol. Soc. London Spec. Publ.*, **73**, 291–319.

Goodall, T.M., **North, C.P.** and **Glennie, K.W.** (2000) Surface and subsurface sedimentary structures produced by salt crusts. *Sedimentology*, **47**, 99–118.

Gradstein, F.M., **Ogg, J.G.** and **van Kranendonk, M.** (2008) On the geologic time scale 2008. *Newsl. Stratigr.*, **43**, 5–13.

Gulliford, A.R., **Flint, S.S.** and **Hodgson, D.M.** (2017) Crevasse splay processes and deposits in an ancient distributive fluvial system: The lower Beaufort Group, South Africa. *Sed. Geol.*, **358**, 1–18.

Hallam, A. and **Wignall, P.B.** (1997) *Mass Extinctions and their Aftermath*. Oxford University Press, Oxford, 332 pp.

Handford, C.R. (1982) Sedimentology and evaporite genesis in a Holocene continental-sabkha playa basin—Bristol Dry Lake, California. *Sedimentology*, **29**, 239–253.

Hejl, E., **Coyle, D.**, **Lal, N.**, **Van den Haute, P.** and **Wagner, G.A.** (1997) Fission-track dating of the western border of the Bohemian massif: thermochronology and tectonic implications. *Geol. Rundsch.*, **86**, 210–219.

Helmkampf, K. (2006) Profilvergleich und sedimentologische Entwicklung im Umkreis der Forschungsbohrungen Spitzeichen 1 und Lindau 1. *Geol. Bavar.*, **109**, 63–94.

Henares, S., **Arribas, J.**, **Cultrone, G.** and **Viseras, C.** (2016a) Muddy and dolomitic rip-up clasts in Triassic fluvial sandstones: Origin and impact on potential reservoir properties (Argana Basin, Morocco). *Sed. Geol.*, **339**, 218–233.

Henares, S., **Bloemsma, M.R.**, **Donselaar, M.E.**, **Mijnlieff, H.F.**, **Redjosentono, A.E.**, **Veldkamp, H.G.** and **Weltje, G.J.** (2014) The role of detrital anhydrite in diagenesis of aeolian sandstones (Upper Rotliegend, The Netherlands): Implications for reservoir-quality prediction. *Sed. Geol.*, **314**, 60–74.

Henares, S., **Caracciolo, L.**, **Viseras, C.**, **Fernández, J.** and **Yeste, L.M.** (2016b) Diagenetic constraints on heterogeneous reservoir quality assessment: A Triassic outcrop analog of meandering fluvial reservoirs. *AAPG Bulletin*, **100**, 1377–1398.

Henares, S., **Donselaar, M.E.** and **Caracciolo, L.** (2020) Depositional controls on sediment properties in dryland rivers: Influence on near-surface diagenesis. *Earth-Sci. Rev.*, **208**, 103297.

Hiete, M., **Berner, U.**, **Heunisch, C.** and **Röhling, H.-G.** (2006) A high-resolution inorganic geochemical profile across the Zechstein-Buntsandstein boundary in the North German Basin. *Z. Dt. Ges. Geowiss.*, **157**, 77–105.

Horton, B.K. and **Schmitt, J.G.** (1996) Sedimentology of a lacustrine fan-delta system, Miocene Horse Camp Formation, Nevada, USA. *Sedimentology*, **43**, 133–155.

Ielpi, A. and **Ghinassi, M.** (2015) Planview style and palaeodrainage of Torridonian channel belts: Applecross Formation, Stoer Peninsula, Scotland. *Sed. Geol.*, **325**, 1–16.

Ingersoll, R.V., **Bullard, T.F.**, **Ford, R.L.**, **Grimm, J.P.**, **Pickle, J.D.** and **Sares, S.W.** (1984) The effect of grain size on detrital modes: a test of the Gazzi-Dickinson point-counting method. *J. Sed. Res.*, **54**, 103–116.

Jewuła, K., **Trela, W.** and **Fijałkowska-Mader, A.** (2020a) Sedimentary and pedogenic record of seasonal humidity during the Permian-Triassic transition on the SE margin of Central European Basin (Holy Cross Mountains, Poland). *Palaeogeogr. Palaeoclimatol. Palaeoecol.*, **564**, 110–154.

Jewuła, K., **Trela, W.** and **Fijałkowska-Mader, A.** (2020b) The Permian-Triassic boundary in continental sedimentary succession at the SE margin of the Central European Basin (Holy Cross Mountains, Poland). *Geol. Mag.*, **157**, 1–14.

Jin, Y.G., **Wang, Y.**, **Wang, W.**, **Shang, Q.H.**, **Cao, C.Q.** and **Erwin, D.H.** (2000) Pattern of marine mass extinction near the Permian-Triassic boundary in South China. *Science*, **289**, 432–436.

Joachimski, M.M., **Alekseev, A.S.**, **Grigoryan, A.** and **Gatovsky, Y.A.** (2020) Siberian Trap volcanism, global warming and the Permian-Triassic mass extinction: New insights from Armenian Permian-Triassic sections. *Geol. Soc. America Bull.*, **132**, 427–443.

Joachimski, M.M., **Lai, X.**, **Shen, S.**, **Jiang, H.**, **Luo, G.**, **Chen, B.**, **Chen, J.** and **Sun, Y.D.** (2012) Climate warming in the latest Permian and the Permian-Triassic mass extinction. *Geology*, **40**, 195–198.

Käsbohrer, F. and **Kuss, J.** (2021) Lower Triassic (Induan) stromatolites and oolites of the Bernburg Formation revisited – microfacies and palaeoenvironment of lacustrine carbonates in Central Germany. *Facies*, **67**, 1–31.

Kearsey, T., **Twitchett, R.J.** and **Newell, A.J.** (2012) The origin and significance of pedogenic dolomite from the Upper Permian of the South Urals of Russia. *Geol. Mag.*, **149**, 291–307.

Kidder, D.L. and **Worsley, T.R.** (2004) Causes and consequences of extreme Permo-Triassic warming to globally equable climate and relation to the Permo-Triassic extinction and recovery. *Palaeogeogr. Palaeoclimatol. Palaeoecol.*, **203**, 207–237.

Klare, B. (1989) *Gliederung und Paläogeographie des Buntsandsteins im Ostteil der Süddeutschen Scholle*. PhD Dissertation. Ruhr-Universität Bochum, Bochum, 150 pp.

Klare, B., **Menzel, D.** and **Schröder, B.** (1995) Fichtelgebirge/ZEV as source areas of Permotriassic alluvial fan deposits. *Contri. 8th Ann KTB Coll.*, **25.5-26.5**, 9–11.

Kutzbach, J.E. and **Gallimore, R.G.** (1989) Pangaean climates: megamonsoons of the megacontinent. *J. Geophys. Res.*, **94**, 3341–3357.

Leeder, M. (1983) On the dynamics of sediment suspension by residual Reynolds stresses—confirmation of Bagnold's theory. *Sedimentology*, **30**, 485–491.

Linnemann, U. (2007) Ediacaran rocks from the Cadomian basement of the Saxo-Thuringian Zone (NE Bohemian Massif, Germany): age constraints, geotectonic setting and basin development. *Geol. Soc. London Spec. Publ.*, **286**, 35–51.

Lowe, D.G. and **Arnott, R.** (2016) Composition and architecture of braided and sheetflood-dominated Ephemeral Fluvial Strata in the Cambrian-Ordovician Potsdam Group: a case example of the morphodynamics of Early Phanerozoic fluvial systems and climate change. *J. Sed. Res.*, **86**, 587–612.

Mack, G.H., **James, W.C.** and **Monger, H.C.** (1993) Classification of paleosols. *Geol. Soc. Am. Bull.*, **105**, 129–136.

Mattern, F. (1995a) Late Carboniferous to early Triassic shear sense reversals at strike-slip faults in eastern Bavaria. *Zbl. Geol. Paläontol.*, **1993**, 1471–1490.

Mattern, F. (1995b) The fault(s) of the "Fränkische Linie" (NE Bavaria), interpreted as a Rotliegend sinistral exstensional strike-slip duplex. *Zentralbl. Geol. Palaontol.*, **1**, 1491–1504.

Meschede, M. and **Warr, L.N.** (2019) *The Geology of Germany*. Springer International Publishing, Cham, 330 pp.

Meyer, R.K.F. (1989) *Die Entwicklung der Pfahl-Störungszone und des Bodenwöhrer Halbgrabens auf Blatt Wackersdorf*. PhD Dissertation. Friedrich-Alexander University Erlangen-Nürnberg, Erlangen, 96 pp.

Miall, A.D. (1977) A review of the braided-river depositional environment. *Earth-Sci. Rev*, **13**, 1–62.

Miall, A.D. (1985) Architectural-Element Analysis: A New Method of Facies Analysis Applied to Fluvial Deposits. *Earth-Sci. Rev*, **22**, 261–308.

Miall, A.D. (2006) *The Geology of Fluvial Deposits. Sedimentary Facies, Basin Analysis, and Petroleum Geology*. 4th Corrected Printing. Springer, Berlin, 599 pp.

Miall, A.D. (2014) *Fluvial Depositional Systems*. Springer International Publishing, Cham, 322 pp.

Minervini, M., **Rossi, M.**, **Mellere, D.**, **Grötsch, J.** and **Gaupp, R.** (2011) Cyclicity and facies relationships at the interaction between aeolian, fluvial, and playa depositional environments in the Upper Rotliegend: regional correlation across UK (Sole Pit Basin), the Netherlands, and Germany. In: *The Permian Rotliegend of the Netherlands* (Eds Grotsch, J. and Gaupp, R.), *SEPM Spec. Publ.*, **98**, 119–146.

Mishra, S., **Aggarwal, N.** and **Jha, N.** (2018) Palaeoenvironmental change across the Permian-Triassic boundary inferred from palynomorph assemblages (Godavari Graben, south India). *Palaeobio. Palaeoenv.*, **98**, 177–204.

Moscariello, A. (2018) Alluvial fans and fluvial fans at the margins of continental sedimentary basins: geomorphic and sedimentological distinction for geo-energy exploration and development. *Geol. Soc. London Spec. Publ.*, **440**, 215–243.

Mulder, T., **Syvitski, J.P.**, **Migeon, S.**, **Faugeres, J.C.** and **Savoye, B.** (2003) Marine hyperpycnal flows: initiation, behavior and related deposits, A review. *Mar. Pet. Geol.*, **20**, 861–882.

Müller, M. (1994) Neue Vorstellungen zur Entwicklung des Nordostbayerischen Permokarbon-Trogs aufgrund reflexionsseismischer Messungen in der Mittleren Oberpfalz. *Geol. Bl. NO-Bayern*, **44**, 195–224.

Nemec, W. and **Steel, R.J.** (1988) What is a fan delta and how do we recognize it? In: *Fan Deltas: Sedimentology and Tectonic Settings* (Eds Nemec, W. and Steel, R.J.), pp. 3–13. Blackie, Glasgow.

Newell, A.J., **Sennikov, A.G.**, **Benton, M.J.**, **Molostovskaya, I.I.**, **Golubev, V.K.**, **Minikh, A.V.** and **Minikh, M.G.** (2010) Disruption of playa–lacustrine depositional systems at the Permo-Triassic boundary: evidence from Vyazniki and Gorokhovets on the Russian Platform. *J. Geol. Soc. London*, **167**, 695–716.

Newell, A.J., **Tverdokhlebov, V.P.** and **Benton, M.J.** (1999) Interplay of tectonics and climate on a transverse fluvial system, Upper Permian, Southern Uralian Foreland Basin, Russia. *Sed. Geol.*, **127**, 11–29.

Nowak, H., **Schneebeli-Hermann, E.** and **Kustatscher, E.** (2019) No mass extinction for land plants at the Permian-Triassic transition. *Nat. Commun.*, **10**, 384.

Olsen, H. (1987) Ancient ephemeral stream deposits: a local terminal fan model from the Bunter Sandstone Formation (L. Triassic) in the Tønder-3, -4 and -5 wells, Denmark. *Geol. Soc. London Spec. Publ.*, **35**, 69–86.

Olsen, H. (1988) The architecture of a sandy braided-meandering river system: an example from the lower Triassic Solling Formation (M. Buntsandstein) in W-Germany. *Geol. Rundsch.*, **77**, 797–814.

Palermo, D., **Aigner, T.**, **Geluk, M.**, **Poeppelreiter, M.** and **Pipping, K.** (2008) Reservoir potential of a lacustrine mixed carbonate/siliciclastic gas reservoir: the lower Triassic Rogenstein in the Netherlands. *J. Petroleum Geol.*, **31**, 61–96.

Parrish, J.T. (1993) Climate of the supercontinent Pangea. *J. Geol.*, **101**, 215–233.

Paul, J.T. (1982) Der Untere Buntsandstein des Germanischen Beckens. *Geol. Rundsch.*, **71**, 795–811.

Paul, J. (2006) Rotliegend und unterer Zechstein der Bohrung Lindau 1 (NE-Bayern). *Geol. Bavar.*, **109**, 27–48.

Péron, S., **Bourquin, S.**, **Fluteau, F.** and **Guillocheau, F.** (2005) Paleoenvironment reconstructions and climate simulations of the Early Triassic: Impact of the water and sediment supply on the preservation of fluvial systems. *Geodin. Acta*, **18**, 431–446.

Peterek, A., **Rauche, H.**, **Schröder, B.**, **Franzke, H.-J.**, **Bankwitz, P.** and **Bankwitz, E.** (1997) The late-and post-Variscan tectonic evolution of the Western Border fault zone of the Bohemian massif (WBZ). *Geol. Rundsch.*, **86**, 191–202.

Pettijohn, F.J., **Potter, P.E.** and **Siever, R.** (1987) Petrography of common sands and sandstones. In: *Sand and Sandstone* (Eds Pettijohn, F.J., Potter, P.E. and Siever, R.), pp. 139–213. Springer, New York, NY.

Renne, P.R., **Black, M.T.**, **Zichao, Z.**, **Richards, M.A.** and **Basu, A.R.** (1995) Synchrony and causal relations between permian-triassic boundary crises and siberian flood volcanism. *Science*, **269**, 1413–1416.

Retallack, G.J. (2013) Permian and Triassic greenhouse crises. *Gondwana Res.*, **24**, 90–103.

Rieke, H.H., **Chilingar, H.** and **George, V.** (1974) *Compaction of Argillaceous Sediments*. Elsevier, New York, 439 pp.

Roscher, M. and **Schneider, J.W.** (2006) Permo-Carboniferous climate: Early Pennsylvanian to Late Permian climate development of central Europe in a regional and global context. *Geol. Soc. London Spec. Publ.*, **265**, 95–136.

Roscher, M., **Stordal, F.** and **Svensen, H.** (2011) The effect of global warming and global cooling on the distribution of

the latest Permian climate zones. *Palaeogeogr. Palaeoclimatol. Palaeoecol.*, **309**, 186–200.

Sarkar, A., **Yoshioka, H.**, **Ebihara, M.** and **Naraoka, H.** (2003) Geochemical and organic carbon isotope studies across the continental Permo-Triassic boundary of Raniganj Basin, eastern India. *Palaeogeogr. Palaeoclimatol. Palaeoecol.*, **191**, 1–14.

Scholze, F., **Wang, X.**, **Kirscher, U.**, **Kraft, J.**, **Schneider, J.W.**, **Götz, A.E.**, **Joachimski, M.M.** and **Bachtadse, V.** (2017) A multistratigraphic approach to pinpoint the Permian-Triassic boundary in continental deposits: The Zechstein-Lower Buntsandstein transition in Germany. *Glob. Planet. Change.*, **152**, 129–151.

Schröder, B. (1987) Inversion tectonics along the western margin of the Bohemian Massif. *Tectonophysics*, **137**, 93–100.

Schröder, B., **Ahrendt, H.**, **Peterek, A.** and **Wemmer, K.** (1997) Post-Variscan sedimentary record of the SW margin of the Bohemian massif: a review. *Geol. Runds.*, **86**, 178–184.

Schuh, H. (1985) Der Zechstein in der Forschungsbohrung Obernsee. *Geol. Bavar.*, **88**, 57–68.

Schumm, S.A. (1985) Patterns of alluvial rivers. *Ann. Rev. Earth Planet. Sci.*, **13**, 5–7.

Siebel, W., **Hann, H.P.**, **Danišík, M.**, **Shang, C.K.**, **Berthold, C.**, **Rohrmüller, J.**, **Wemmer, K.** and **Evans, N.J.** (2010) Age constraints on faulting and fault reactivation: a multi-chronological approach. *Int. J. Earth Sci.*, **99**, 1187–1197.

Słowakiewicz, M., **Tucker, M.E.**, **Pancost, R.D.**, **Perri, E.** and **Mawson, M.** (2013) Upper Permian (Zechstein) microbialites: Supratidal through deep subtidal deposition, source rock, and reservoir potential. *AAPG Bulletin*, **97**, 1921–1936.

Smith, R.M.H. (1995) Changing fluvial environments across the Permian-Triassic boundary in the Karoo Basin, South Africa and possible causes of tetrapod extinctions. *Palaeobio. Palaeoenv.*, **117**, 81–104.

Smoot, J.P. and **Castens-Seidell, B.** (1994) Sedimentary features produced by efflorescent salt crusts, Saline Valley and Death Valley, California. In: *Sedimentology and Geochemistry of Modern and Ancient Saline Lakes* (Eds Renaut, R.W. and Last, W.M.), *SEPM Spec. Publ.* **50**, 73–90.

Soffel, H.C. and **Wippern, J.** (1998) Magnetostratigraphy of Upper Permian and Lower Triassic Rocks from the Drill Site Obernsees near Bayreuth, Germany. *Geol. Bavar.*, **103**, 275–294.

Song, H., **Wignall, P.B.**, **Tong, J.** and **Yin, H.** (2013) Two pulses of extinction during the Permian-Triassic crisis. *Nat. Geosci.*, **6**, 52–56.

Soria, J.M., **Fernández, J.**, **García, F.** and **Viseras, C.** (2003) Correlative low stand deltaic and shelf systems in the Guadix Basin (Late Miocene, Betic Cordillera, Spain): the stratigraphic record of forced and normal regressions. *J. Sed. Res.*, **73**, 912–925.

Stanistreet, I.G. and **McCarthy, T.S.** (1993) The Okavango Fan and the classification of subaerial fan systems. *Sed. Geol.*, **85**, 115–133.

Stanistreet, I.G. and **Stollhofen, H.** (2002) Hoanib River flood deposits of Namib Desert interdunes asanalogues for thin permeability barrier mudstone layers in aeolianite reservoirs. *Sedimentology*, **49**, 719–736.

Stollhofen, H., **Bachmann, G.H.**, **Barnasch, J.**, **Bayer, U.**, **Beutler, G.**, **Franz, K.M.**, **Legler, B.**, **Mutterlose, J.** and **Radies, D.** (2008) Upper Rotliegend to Early Cretaceous basin development. In: *Dynamics of Complex Intracontinental Basins: The Example of the Central European Basin System* (Eds Littke, R., Bayer, U., Gajewski, D. and Nelskamp, S.), pp. 156–245. Springer, Berlin.

Stollhofen, H. and **Stanistreet, I.G.** (1994) Interaction between bimodal volcanism, fluvial sedimentation and basin development in the Permo-Carboniferous Saar-Nahe Basin (south-west Germany). *Basin Res.*, **6**, 245–267.

Summerhayes, C.P. (2015) *Earth's Climate Evolution*. John Wiley & Sons, Chichester West Sussex and Hoboken, NJ, 394 pp.

Sun, Y.D., **Joachimski, M.M.**, **Wignall, P.B.**, **Yan, C.**, **Chen, Y.**, **Jiang, H.**, **Wang, L.** and **Lai, X.** (2012) Lethally hot temperatures during the Early Triassic greenhouse. *Science*, **338**, 366–370.

Svendsen, J., **Stollhofen, H.**, **Krapf, C.B.** and **Stanistreet, I.G.** (2003) Mass and hyperconcentrated flow deposits record dune damming and catastrophic breakthrough of ephemeral rivers, Skeleton Coast Erg, Namibia. *Sed. Geol.*, **160**, 7–31.

Swan, A., **Hartley, A.J.**, **Owen, A.** and **Howell, J.** (2018) Reconstruction of a sandy point-bar deposit: implications for fluvial facies analysis. *Int. Assoc. Sedimentol. Spec. Publ.*, **48**, 445–474.

Szurlies, M. (2007) Latest Permian to Middle Triassic cyclo-magnetostratigraphy from the Central European Basin, Germany: Implications for the geomagnetic polarity timescale. *Earth Planet. Sci. Lett.*, **261**, 602–619.

Tabor, N.J., **Myers, T.S.** and **Michel, L.A.** (2017) Sedimentologist's guide for recognition, description, and classification of paleosols. In: *Terrestrial Depositional Systems* (Eds Ziegler, K.E. and Parker, W.), pp. 165–208. Elsevier, Amsterdam.

Tan, M., **Zhu, X.**, **Wei, W.**, **Wu, C.** and **Pan, R.** (2018) The sequence stratigraphy and depositional characteristics of fan-delta complexes in the Upper Bayingebi Member (Lower Cretaceous) in Chagan Sag, Inner Mongolia, China. *Geol. J.*, **53**, 349–370.

Tucker, M.E. (1991) Sequence stratigraphy of carbonate-evaporite basins: models and application to the Upper Permian (Zechstein) of northeast England and adjoining North Sea. *J. Geol. Soc. London*, **148**, 1019–1036.

Vermeesch, P., **Resentini, A.** and **Garzanti, E.** (2016) An R package for statistical provenance analysis. *Sed. Geol.*, **336**, 14–25.

Viglietti, P.A., **Rubidge, B.S.** and **Smith, R.M.H.** (2017) New Late Permian tectonic model for South Africa's Karoo Basin: foreland tectonics and climate change before the end-Permian crisis. *Sci. Rep.*, **7**, 1–7.

Viseras, C. and **Fernández, J.** (1994) Channel migration patterns and related sequences in some alluvial fan systems. *Sed. Geol.*, **88**, 201–217.

Viseras, C., **Henares, S.**, **Yeste, L.M.** and **García-García, F.** (2018) Reconstructing the architecture of ancient meander belts by compiling outcrop and subsurface data: A Triassic example. Meandering Rivers. *IAS, Spec. Public.*, **48**, 419–444.

Viseras, C., **Soria, J.M.**, **Durán, J.J.**, **Pla, S.**, **Garrido, G.**, **García-García, F.** and **Arribas, A.** (2006) A large-mammal site in a meandering fluvial context (Fonelas P-1, Late Pliocene, Guadix Basin, Spain): Sedimentological keys for its paleoenvironmental reconstruction. *Palaeogeogr. Palaeoclimatol. Palaeoecol.*, **242**, 139–168.

Voigt, T., **Gaupp, R.** and **Rohling, H.** (2011) Lake deposits of the Early Triassic Buntsandstein in Central Germany: Type localities of oolites and stromatolites. In: *5th International*

Limnogeological Congress, Konstanz, Abstract Volume and Field Guide, Constanza, 191–211.

Walker, R.G. (1984) *Facies Models* (2nd edn). Geological Association of Canada, St. John, NL, 317 pp.

de Wall, H., **Schaarschmidt, A.**, **Kämmlein, M.**, **Gabriel, G.**, **Bestmann, M.** and **Scharfenberg, L.** (2019) Subsurface granites in the Franconian Basin as the source of enhanced geothermal gradients: a key study from gravity and thermal modeling of the Bayreuth Granite. *Int. J. Earth. Sci.*, **108**, 1913–1936.

Ward, P.D., **Montgomery, D.R.** and **Smith, R.** (2000) Altered river morphology in south Africa related to the permian-triassic extinction. *Science*, **289**, 1740–1743.

Warren, J. (2000) Dolomite: occurrence, evolution and economically important associations. *Earth-Sci. Rev*, **52**, 1–81.

Warren, J.K. (2006) *Evaporites. Sediments, Resources, and Hydrocarbons*. Springer, Berlin, 1036 pp.

Weber, K.I. (1993) Paleosols in Triassic sediments of Southeast Germany (Bavaria). *Bull. N. M. Mus. Nat. Hist. Sci.*, **3**, 477–478.

Yeste, L.M., **Varela, A.N.**, **Viseras, C.**, **Mcdougall, N.D.** and **García-García, F.** (2020) Reservoir architecture and heterogeneity distribution in floodplain sandstones: Key features in outcrop, core and wireline logs. *Sedimentology*, **67**, 3355–3388.

Žák, J., **Verner, K.**, **Finger, F.**, **Faryad, S.W.**, **Chlupáčová, M.** and **Veselovský, F.** (2011) The generation of voluminous S-type granites in the Moldanubian unit, Bohemian Massif, by rapid isothermal exhumation of the metapelitic middle crust. *Lithos*, **121**, 25–40.

Zhu, Z., **Kuang, H.**, **Liu, Y.**, **Benton, M.J.**, **Newell, A.J.**, **Xu, H.**, **An, W.**, **Ji, S.**, **Xu, S.**, **Peng, N.** and **Zhai, Q.** (2020) Intensifying aeolian activity following the end-Permian mass extinction: Evidence from the Late Permian-Early Triassic terrestrial sedimentary record of the Ordos Basin, North China. *Sedimentology*, **67**, 2691–2720.

Ziegler, P.A. (1990) *Geological Atlas of Western and Central Europe*. Geological Society of London, London, 239 pp.

Zuffa, G.G. (1985) *Optical Analyses of Arenites: Influence of Methodology on Compositional Results*. Springer, Dordrecht, 25 pp.

Zulauf, G. (1993) Brittle deformation events at the western border of the Bohemian Massif (Germany). *Geol. Rundsch.*, **82**, 489–504.

van der Zwan, C.J. and **Spaak, P.** (1992) Lower to Middle Triassic sequence stratigraphy and climatology of the Netherlands, a model. *Palaeogeogr. Palaeoclimatol. Palaeoecol.*, **91**, 277–290.

Manuscript received 30 October 2020; revision accepted 23 June 2021

Supporting Information

Additional information may be found in the online version of this article:

Table S1. Detailed pointcount results.

